CASE STUDIES OF THE CIRCULAR RESTRICTED THREE BODY PROBLEM

by

WILLIAM JASON EBERLE

Presented to the Faculty of the Graduate School of

The University of Texas at Arlington in Partial Fulfillment

of the Requirements

for the Degree of

MASTER OF SCIENCE IN PHYSICS

THE UNIVERSITY OF TEXAS AT ARLINGTON

May 2007

To the memory of my grandfather William Jacob Eberle.

ACKNOWLEDGEMENTS

I would like to thank my supervising professor Dr. Manfred Cuntz for constantly motivating and encouraging me, and also for his invaluable advice during the course of my studies. I wish to thank my academic advisors Dr. Zdzislaw Musielak and Dr. John Fry for their interest in my research and for taking time to serve in my committee.

I would also like to express my deep gratitude to my parents, Kip and Darlene Eberle, without whom I wouldn't even be alive. They have motivated me and made many sacrifices to provide me with opportunities that they didn't have. I am very fortunate to be so blessed. I am also extremely grateful to my wife Sarinya for her encouragement and patience. I also want to thank my sisters Sandy and Nikki for their perspectives that have helped to develop mine.

Finally, I want to acknowledge all of my friends and acquaintances that I have known throughout my education. I am especially indebted to Marcus Hawkins for providing me with a sounding board and introducing me to new concepts while I discovered my interest in physics.

April 19, 2007

ABSTRACT

CASE STUDIES OF THE CIRCULAR RESTRICTED THREE BODY PROBLEM

Publication No. _____

William Jason Eberle, M.S.

The University of Texas at Arlington, 2007

Supervising Professor: Manfred Cuntz

In this thesis, the onset of instability for a planet which is part of a stellar binary system is investigated by performing numerical simulations of the circular restricted three body problem. This study also makes use of a rotating (synodic) coordinate system keeping both binary stars at rest. This allows the definition of a constant of motion (Jacobi's constant), which in turn sets a permissible region of motion for the planet. As the initial conditions are varied, the boundary of the permissible region of motion passes through each of the three collinear equilibrium points with significant changes to the orbit of the planet at or near each crossing. The synodic velocity phase space portraits are also used in order to obtain the average eccentricity of the orbit as an additional means of determining the stability. The stability limits obtained via these methods agree with other methods that were obtained with simulations over much longer time intervals.

TABLE OF CONTENTS

LIST OF FIGURES

LIST OF TABLES

CHAPTER 1

INTRODUCTION

Ever since the foundation of Newton's mechanics in 1687, the general problem of finding a closed form solution for the motion of $N > 2$ bodies under their mutual gravitation has remained intractable. This is somewhat famously known as the N-Body problem. More specifically, the three-body problem ($N = 3$) has been investigated extensively over the last three centuries. With specific assumptions, a handful of closed form solutions have been found. Some of these solutions are stable, while others are unstable. For example, three equal masses orbiting about their common center of mass at the vertices of an equilateral triangle is unstable while three equal masses moving in a figure eight pattern is stable as shown in Chenciner and Montgomery (2000). Unlike the case with two bodies, the three body problem has no simple *general* solution that can be written down to describe the motion for all time for any arbitrary initial conditions and it was proven that this was the case by Henri Poincaré in 1887.

Considering the case where one of the masses is very small compared to the other two reduces the complexity of the problem by allowing us to disregard the accelerations of the larger masses due to the interaction with the small one. The two large masses then just follow orbits about each other determined by their mutual gravitational attraction. The problem remains to determine the motion of the small mass in the vicinity of the two large masses. This is what is known as the restricted three body problem, and this model can be used to study some great problems. For example, studying a satellite moving within the Earth-Moon system was essential in making the Apollo missions a success. The question of whether or not the Moon will remain in an orbit around the

Earth can be understood from the perspective of the Sun-Earth system with the Moon as the small mass. Even the very history and future of life on Earth could be connected with such a seemingly simple model. Now, the hunt is on for planets orbiting distant stars, and we come back to this centuries old problem to try to determine where these extra-solar planets can exist.

As of April 20^{th} 2007, http://exoplanet.eu/ lists the total number of extra-solar planets discovered is 227, and planets with a mass less then 2 times Jupiter's mass make up just over 59% of the population. See Fig. 1.1. No Earth mass planets have been discovered yet, but the distribution of mass for extra-solar planets would seem to indicate that there is a swarm of terrestrial planets out there; we just have to be patient until we have the technology to detect them.

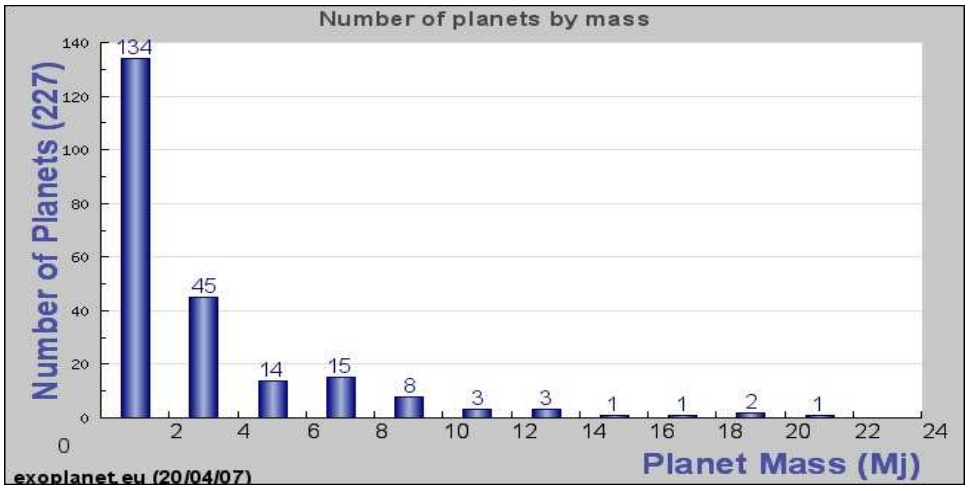

Figure 1.1. Mass distribution of extra solar planets.

NASA and the European Space Agency are working on a new breed of interferometer arrays that will take up positions in stable points in the solar system looking for evidence of *terrestrial* sized planets around other stars. These detectors, NASA's

Terrestrial Planet Finder, T.P.F. and ESA's Darwin, if approved, should be operational within the coming decades.

The search for extra-solar planets has primarily focused on solitary stars because finding planets around binary stars is more difficult. But Duquennoy and Mayor (1991) showed that most Sun like stars are in binary or multiple systems. If most Sun-like stars in this region of the galaxy are a part of a multi-star system, then how likely is it that these systems have planets with stable orbits? This is a very difficult question to answer and the only way to really answer it is to observe actual systems to obtain statistics on what is really out there. Theoretical studies such as those conducted by Kley (2001) and Quintana et al. (2002) showed that planets can successfully form in binary (and possibly multiple) stellar systems, albeit the predominant effect of a companion on the efficiency of planet formation appeared to be a negative one. Unequivocal observational evidence for the existence of planets in binary (and higher order) systems was given by Patience et al. (2002), Eggenberger et al. (2004), Konacki (2005), Bakos et al. (2007), and others. Bonavita and Desidera (2007) performed a statistical analysis for binaries and multiple systems concerning the frequency of planets, and concluded that there is no statistical difference between those systems and single stars. That planets in binary systems are now assumed to be relatively common is also implied by the recent detection of debris disks in many main-sequence stellar binary systems using the *Spitzer Space Telescope* (e.g., Trilling et al. 2007). Out of an observed 69 A3-F8 main sequence binary star systems, nearly 60% showed dust disks surrounding binary stars with a separation less than 3 A.U. For the wide binary separations, 50 - 500 A.U., approximately 45% were found to have disks orbiting the primary star. The intermediate binary separations showed no evidence of debris disks.

In the last few decades, significant progress has been made in the study of orbital stability of planets in binary systems. Most of these studies focus on S-type systems,

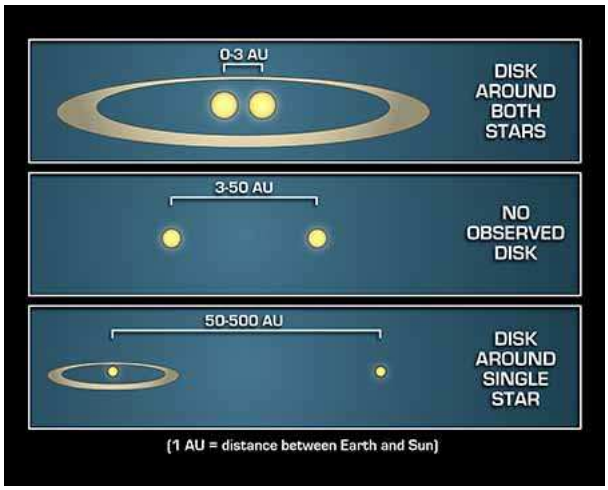

Figure 1.2. Dust disks around binary star systems found by the Spitzer Space Telescope. Credit: NASA/JPL-Caltech/T. Pyle (SSC).

where the planet is orbiting one of the stars with the second star to be considered a source of perturbations. Early results have been obtained by Dvorak (1986) and Holman and Wiegert (1999); which explore the long-term stability of planets in binary systems for different mass ratios and binary eccentricities. More recently, David et al. (2003) investigated the orbital stability of an Earth-mass planet around a solar-mass star in the presence of a companion star. They determined the planet's ejection time for systems with a variety of orbital eccentricities and semi-major axes. For fixed companion masses, the ejection time was found to be a steep function of the periastron distance (or orbital radius for circular orbits) to the primary star, a prediction that is consistent with subsequent results by Musielak et al. (2005). They also deduced orbital stability limits for planets, which were found to depend on the stellar mass ratios, a result, which will be further explored in this thesis.

More recent results on planetary orbital stability in binary systems have been obtained by Mudryk and Wu (2006) and Fatuzzo et al. (2006). The first paper focuses on the role of resonances in the ejection of planets. The second paper supplies a detailed

statistical analysis of ejection times in response to a large number of configurations, both concerning the planet and the companion star. In this paper we will present criteria for the orbital stability of planets in binary systems based on Jacobi's integral and constant as well as on a statistical analysis of planetary orbital eccentricity in the synodic coordinate system.

In our theoretical investigation the following assumptions concerning the makeup of the binary system containing a planet are introduced:

1. The stars initially orbit each other in circles.
2. The orbit of the planet is in the same orbital plane as the binary stars and it is initially to the right of the primary star along the line joining the binary stars. (3 o'clock position)
3. The planet has an initial velocity that results in a counter clockwise circular orbit about the primary star.
4. The mass of the planet is 1×10^{-6} the mass of the star it orbits.

The first assumption greatly simplifies the problem because we can introduce a coordinate system in which the binary stars remain at rest. It is an oversimplification because it is impossible for any given binary system to be perfectly circular. Trying to treat the more general case of elliptical binaries would be more desirable, but also much more difficult. For example, a rotating coordinate system will not have fixed positions for stars orbiting in ellipses. Since we are also assuming that the planet has a very small mass compared to the stars, the acceleration of the stars due to the gravitational force of the planet will be minuscule and their orbits will not be significantly affected.

Assuming that the planet is orbiting in the same plane as the binary system is perhaps less arbitrary since the planets in our own solar system are all within 7° of Earth's orbital plane. The specification that the planet starts in the 3 o'clock position is just a matter of preference. The initial position could just as well be chosen to be at

6 o'clock or even 9:30, but the 3 o'clock position has the benefit of simplifying certain analytical expressions later on.

The third assumption is based on the idea that when a star forms, the debris left over is all rotating in the same direction as the rotation of the star. There is not yet a definitive way to specify which way a star in a binary system is rotating, so it was tacitly assumed that the primary star is rotating counterclockwise which would result in the planet's orbit being counterclockwise as well. It could be possible that the star would be rotating in the opposite direction and the planet would have a retrograde orbit. Furthermore, the star could be rotating with an axis that is not perfectly perpendicular to the binary orbital plane at all. These complications are worth investigating, but once again, the investigation would have been too difficult.

Finally the last assumption comes from the fact that the ratio of the Earth's mass, $M_{\oplus}$, to the Sun's mass, $M_{\odot}$ in kilograms is $M_{\oplus}/M_{\odot} = 5.97 \times 10^{24}$ kg$/2.99 \times 10^{30}$ kg $\approx 3 \times 10^{-6}$.

More specifically, the setup for the system of study is a binary system where the total mass of the stars is $10M_{\odot}$, and the separation between them is 10 A.U. From Kepler's third law, this results in a binary period that is always 10 years. The bulk of the simulations that were run spanned a simulated time of 50 years, which of course means that only 5 binary periods elapse during the course of the simulation. Some initial conditions were carried out for a 1000-year simulation time, which amounts to 100 binary periods. In either case this is inadequate to determine long-term stability of a planet in a binary system. As a matter of perspective, the time scale for the chaotic behavior in our Solar System has been shown to be on the order of millions of years by Sussman and Wisdom (1992), as well as Laskar (2002). Therefore, a discussion of long-term stability is beyond the scope of this thesis. However, we do have promising results indicating where the instability sets in within a short time interval based on analytical considerations

and the results obtained would likely shift if time scales of millions of years were to be considered.

As a last note on the applicability of the contents of this work, the reader should be aware that the particular parameters chosen for the total mass of the binary stars and the separation between them need not be so specific, and the results obtained in the following will scale to any circular binary system with the most dramatic effect on the orbital period of the system. For example, if while maintaining a separation of 10 A.U., we were to choose a mass of $1M_{\odot}$ for the primary star and a mass of $xM_{\odot}$, where $0 < x < 1$, for the secondary star, instead of a total mass of $10M_{\odot}$, the period of binary orbits would be between 3.162 and 2.236 times longer than what is considered here. The nature of the orbit of the planet would be the same for a given set of initial conditions but the time dependent development would take place at slower rate.

CHAPTER 2

BASIC THEORY

2.1 System setup with definitions and basic equations

In general, the two stars can move relative to one another in any form of a conic section; for example, ellipse, parabola or hyperbola. Only elliptical paths are closed and are considered as orbits. The circular orbit is a special case of elliptical orbits and that is what is considered in the following. The origin of the coordinate system is chosen

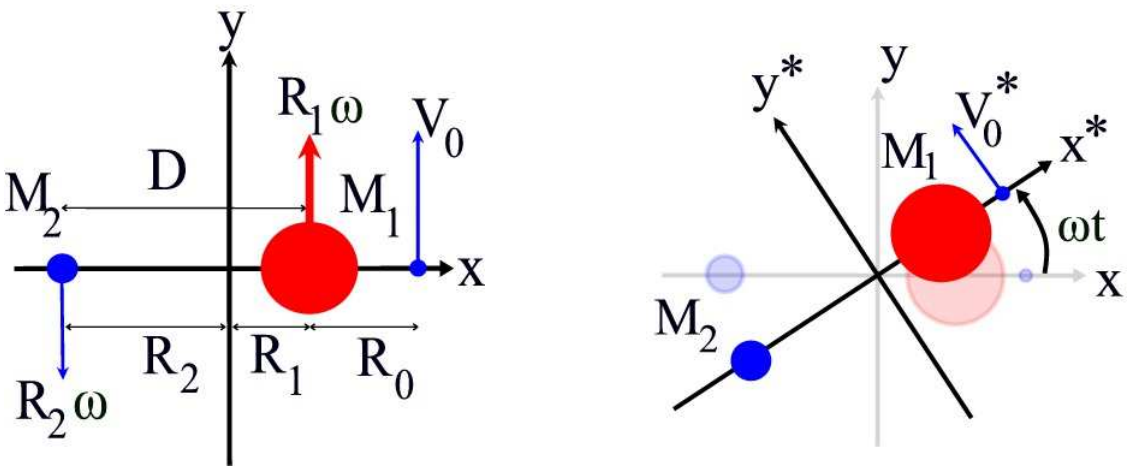

(a) (b)

Figure 2.1. Basic setup used for circular restricted three body problem. (a) Initial conditions in sidereal coordinates. (b) Relationship to synodic coordinates.

at the center of mass of the two binary stars. Therefore, we find

$$M_1 R_1 = M_2 R_2 \tag{2.1}$$

with index 1 referring to the star of greater or equal mass, placed to the right, and index 2 referring to the star placed to the left in all forthcoming figures. All quantities are assumed to have their usual meaning, unless noted otherwise. The basic setup is depicted in Fig. 2.1. The motion of the binary stars is taken to be circular so by equating the gravitational force to the centripetal force on each star we have

$$\frac{GM_1M_2}{D^2} = \frac{M_1{V_1}^2}{R_1} = \frac{M_2{V_2}^2}{R_2} \tag{2.2}$$

where $D = R_1 + R_2$. Since the velocity for circular motion can be expressed as $V_i = R_i\omega$ for $i = 1, 2$ with ω as the angular velocity of the system, and V_i as velocity of star i relative to the center of mass, we can find:

$$V_i^2 \;=\; R_i\frac{GM_j}{D^2} \;=\; R_i^2\omega^2 \tag{2.3}$$

with $j = 3 - i$. Or

$$\omega^2 = \frac{M_j}{R_i}\frac{G}{D^2} \tag{2.4}$$

Now then, because of (2.1):

$$M_1 + M_2 = M_j(1 + \frac{R_j}{R_i}) \tag{2.5}$$

It is then easy to show that:

$$\frac{M_j}{R_i} = \frac{M_1 + M_2}{D} = \frac{M}{D} \tag{2.6}$$

where now $M = M_1 + M_2$ is the combined mass of stars 1 and 2. Substituting this back into equation (2.4); we obtain

$$\omega^2 = \frac{GM}{D^3} \tag{2.7}$$

which is Kepler's third law.

The relative size of the two stars in the binary system has a significant affect on the regions of stability for the planet. There are several ways to quantify this mass ratio such

as taking the smaller mass divided by the larger mass. We will however define the mass ratio as the mass of the smaller star divided by the total mass of both stars; $\mu = \frac{M_2}{M}$. With $\alpha = 1 - \mu$ we obtain the mass and position of the two stars in terms of the mass ratio, the total mass of the binary stars, and the distance between them:

$$M_1 = \alpha M \qquad R_1 = \mu D \qquad M_2 = \mu M \qquad R_2 = \alpha D$$

2.2 Equations of motion in fixed (Sidereal) coordinates

The following derivation of the equations of motion loosely follows chapter one from Szebehely (1967). Similar information can be found in Symon (1971), and Roy (2005). Since we are assuming the binary stars have circular motion, the positions of star 1 and 2, as functions of time t, denoted as $X_1(t)$, $Y_1(t)$, $X_2(t)$ and $Y_2(t)$, are given as

$$\begin{aligned} X_1(t) &= \mu D \cos \omega t \quad \text{and} \quad Y_1(t) = \mu D \sin \omega t \\ X_2(t) &= -\alpha D \cos \omega t \quad \text{and} \quad Y_2(t) = -\alpha D \sin \omega t \end{aligned} \tag{2.8}$$

We are also considering a small planet with mass m_3 subject to the gravity of both stars. The distance of the small object to star $i = 1,\ 2$ is given as $r_i(t) = [(X_3(t) - X_i(t))^2 + (Y_3(t) - Y_i(t))^2]^{\frac{1}{2}}$, with X_3 and Y_3 as (sidereal) coordinates of the small object. The potential energy of the small object is given as

$$U_3 = -\frac{GM_1 m_3}{r_1} - \frac{GM_2 m_3}{r_2}. \tag{2.9}$$

The planet's acceleration vector $\boldsymbol{a_3}$ is

$$\boldsymbol{a_3} = \frac{1}{m_3}\boldsymbol{F_3} = -\frac{1}{m_3}\boldsymbol{\nabla_3} U_3 \tag{2.10}$$

where $\boldsymbol{F_3}$ is the force acting on the planet and $\boldsymbol{\nabla_3} = <\frac{\partial}{\partial X_3},\ \frac{\partial}{\partial Y_3}>$ is the gradient operator acting on the coordinates of the planet. We thus obtain

$$\begin{aligned} \ddot{X}_3 &= -\frac{GM_1}{{r_1}^3}(X_3 - X_1) - \frac{GM_2}{{r_2}^3}(X_3 - X_2) \\ \ddot{Y}_3 &= -\frac{GM_1}{{r_1}^3}(Y_3 - Y_1) - \frac{GM_2}{{r_2}^3}(Y_3 - Y_2)\ . \end{aligned} \tag{2.11}$$

2.3 Introducing dimensionless coordinates

The distance D between the binary stars will be useful as a scale factor to put distances into a dimensionless form based on the substitutions $X_3 = Dx_3$ and $Y_3 = Dy_3$. Thus, the dimensionless position vector for the small mass in the sidereal reference frame is given as $<x_3,\ y_3>$. We also introduce a dimensionless time τ as $\tau = \omega t$. The dimensionless representation of the velocity, $<\dot{x}_3,\ \dot{y}_3>$, and acceleration, $<\ddot{x}_3,\ \ddot{y}_3>$, for the planet can be found from $dX_3/dt = D\omega\dot{x}_3$ and $d^2X_3/dt^2 = D\omega^2\ddot{x}_3$, respectively. Equivalent equations hold for the variables in the y direction and the overdot represents differentiation with respect to the dimensionless time τ. Upon substitution of these quantities into (2.11), we find

$$\begin{aligned} \ddot{x}_3 &= -\left(\frac{\alpha}{{r_1}^3}(x_3 - \mu\cos\tau) + \frac{\mu}{{r_2}^3}(x_3 + \alpha\cos\tau)\right) \\ \ddot{y}_3 &= -\left(\frac{\alpha}{{r_1}^3}(y_3 - \mu\sin\tau) + \frac{\mu}{{r_2}^3}(y_3 + \alpha\sin\tau)\right) \end{aligned} \tag{2.12}$$

with

$$\begin{aligned} r_1(t) &= [(x_3(t) - \mu\cos\tau)^2 + (y_3(t) - \mu\sin\tau)^2]^{\frac{1}{2}} \\ r_2(t) &= [(x_3(t) + \alpha\cos\tau)^2 + (y_3(t) + \alpha\cos\tau)^2]^{\frac{1}{2}}\ . \end{aligned} \tag{2.13}$$

This set of equations constitutes the dimensionless form of the equations of motion using fixed (sidereal) coordinates.

2.4 Transforming to Rotating (Synodic) coordinates

Next we transform the equations of motion (see Eq. 2.12) into a rotating (synodic) coordinate system that rotates along with the binary stars. Since the binary stars are orbiting each other counterclockwise, the necessary transformation is a rotation in the counterclockwise direction such that the binary stars remain at fixed positions which simplifies the restricted three body problem. In addition, fixed equilibrium points (Lagrange points) can be found at which the small mass rotates in sync with the binary stars. These will be discussed further in § 3.2

The vector transformation between the sidereal $\boldsymbol{V}$ and the synodic coordinate system $\boldsymbol{V^*}$ involves multiplication by the rotation matrix $\mathbf{R}$ and inverse matrix $\mathbf{R}^{-1}$, respectively, according to $\boldsymbol{V^*} = \mathbf{R}\boldsymbol{V}$ and $\boldsymbol{V} = \mathbf{R}^{-1}\boldsymbol{V^*}$, with the two matrices given as

$$\mathbf{R} = \begin{bmatrix} \cos\tau & \sin\tau \\ -\sin\tau & \cos\tau \end{bmatrix} \qquad \textbf{and} \qquad \mathbf{R}^{-1} = \begin{bmatrix} \cos\tau & -\sin\tau \\ \sin\tau & \cos\tau \end{bmatrix}.$$

Thus, the position of the binary stars and the planet in dimensionless synodic coordinates are given as

$$\begin{aligned}
\begin{bmatrix} x_1^* \\ y_1^* \end{bmatrix} &= \mathbf{R} \begin{bmatrix} x_1 \\ y_1 \end{bmatrix} = \mathbf{R} \begin{bmatrix} \mu\cos\tau \\ \mu\sin\tau \end{bmatrix} = \begin{bmatrix} \mu \\ 0 \end{bmatrix} \\
\begin{bmatrix} x_2^* \\ y_2^* \end{bmatrix} &= \mathbf{R} \begin{bmatrix} x_2 \\ y_2 \end{bmatrix} = \mathbf{R} \begin{bmatrix} -\alpha\cos\tau \\ -\alpha\sin\tau \end{bmatrix} = \begin{bmatrix} -\alpha \\ 0 \end{bmatrix} \\
\begin{bmatrix} x_3^* \\ y_3^* \end{bmatrix} &= \mathbf{R} \begin{bmatrix} x_3 \\ y_3 \end{bmatrix} = \begin{bmatrix} x_3\cos\tau + y_3\sin\tau \\ -x_3\sin\tau + y_3\cos\tau \end{bmatrix} .
\end{aligned} \tag{2.14}$$

The latter equation can also be used to obtain relationships for the position, velocity and acceleration of the small mass in the two frames of reference

$$\begin{aligned}
\begin{bmatrix} x_3 \\ y_3 \end{bmatrix} &= \mathbf{R}^{-1} \begin{bmatrix} x_3^* \\ y_3^* \end{bmatrix} = \begin{bmatrix} x_3^*\cos\tau - y_3^*\sin\tau \\ x_3^*\sin\tau + y_3^*\cos\tau \end{bmatrix} \\
\begin{bmatrix} \dot{x}_3 \\ \dot{y}_3 \end{bmatrix} &= \mathbf{R}^{-1} \begin{bmatrix} \dot{x}_3^* - y_3^* \\ \dot{y}_3^* + x_3^* \end{bmatrix} \\
\begin{bmatrix} \ddot{x}_3 \\ \ddot{y}_3 \end{bmatrix} &= \mathbf{R}^{-1} \begin{bmatrix} \ddot{x}_3^* - 2\dot{y}_3^* - x_3^* \\ \ddot{y}_3^* + 2\dot{x}_3^* - y_3^* \end{bmatrix}
\end{aligned} \tag{2.15}$$

By multiplying both sides of Eq. (2.12) by $\mathbf{R}$ and using the above relations we obtain the equations of motion in the synodic coordinate system. If we label all the components of position, velocity, and acceleration in the synodic frame by an asterisk $(*)$, we find

$$\begin{aligned}
\ddot{x}_3^* - 2\dot{y}_3^* &= x_3^* - \frac{\alpha}{{r_1}^3}(x_3^* - \mu) - \frac{\mu}{{r_2}^3}(x_3^* + \alpha) \\
\ddot{y}_3^* + 2\dot{x}_3^* &= (1 - \frac{\alpha}{{r_1}^3} - \frac{\mu}{{r_2}^3})y_3^*
\end{aligned} \tag{2.16}$$

where the dimensionless distances to each star can now be expressed as

$$\begin{aligned} r_1(t) &= [(x_3^*(t)-\mu)^2 + y_3^*(t)^2]^{\frac{1}{2}} \\ r_2(t) &= [(x_3^*(t)+\alpha)^2 + y_3^*(t)^2]^{\frac{1}{2}} \ . \end{aligned} \tag{2.17}$$

CHAPTER 3

JACOBI'S INTEGRAL AND CONSTANT

3.1 Derivation of Jacobi's integral

The components on the right side of Eqs. (2.16) are accelerations in the non-inertial reference frame of the rotating binary system. These can be rewritten as forces per unit mass or as the gradient of a scaler pseudo-potential $\overline{\phi}$, leading to

$$x_3^* - \frac{\alpha}{{r_1}^3}(x_3^* - \mu) - \frac{\mu}{{r_2}^3}(x_3^* + \alpha) \quad = \quad \frac{\partial \overline{\phi}}{\partial x_3^*} \tag{3.1}$$

$$y_3^*(1 - \frac{\alpha}{{r_1}^3} - \frac{\mu}{{r_2}^3}) \quad = \quad \frac{\partial \overline{\phi}}{\partial y_3^*} \ , \tag{3.2}$$

which is satisfied by

$$\overline{\phi} \ = \ \frac{1}{2}\left[\left(x_3^{*2} + y_3^{*2}\right) + 2\left(\frac{\alpha}{r_1} + \frac{\mu}{r_2}\right)\right] \ . \tag{3.3}$$

Now Eqs. (2.16) can be expressed as

$$\ddot{x}_3^* \dot{x}_3^* + \ddot{y}_3^* \dot{y}_3^* \ = \ \frac{\partial \overline{\phi}}{\partial x_3^*}\dot{x}_3^* + \frac{\partial \overline{\phi}}{\partial y_3^*}\dot{y}_3^* \ , \tag{3.4}$$

which if integrated with respect to τ leads to

$$\frac{1}{2}\left(\dot{x}_3^{*2} + \dot{y}_3^{*2}\right) \ = \ \overline{\phi} - \frac{\overline{C}}{2} \tag{3.5}$$

where $\overline{C}$ constitutes a constant of integration.

For the small mass the dimensionless distance from the center of mass and the synodic velocity are

$$\begin{aligned} r(\tau) \quad &= \quad [x_3^{*2}(\tau) + y_3^{*2}(\tau)]^{\frac{1}{2}} \\ v^*(\tau) \quad &= \quad [\dot{x}_3^{*2}(\tau) + \dot{y}_3^{*2}(\tau)]^{\frac{1}{2}} \ , \end{aligned} \tag{3.6}$$

which allow us to rewrite Eq. (3.5) as

$$v^{*2} \;=\; 2\overline{\phi} - \overline{C} \;=\; r^2 + 2\left(\frac{\alpha}{r_1} + \frac{\mu}{r_2}\right) - \overline{C}\;. \tag{3.7}$$

This is an integral of motion in the rotating cartesian coordinate system known as Jacobi's integral.

3.2 Lagrange points

At this point in the development, it is beneficial to discuss a few useful solutions to Eqs. (3.1) and (3.2). If we consider the situation when the net force acting on the planet is zero, including centrifugal fictitious forces due to the rotation of the non-inertial synodic reference frame, then the planet will have zero acceleration in that frame and we will have an equilibrium position. Thus if the planet were to be placed exactly at such a point, then it would remain there. As such, Eqs. (3.1) and (3.2) would become

$$x_3^* - \frac{\alpha}{{r_1}^3}(x_3^* - \mu) - \frac{\mu}{{r_2}^3}(x_3^* + \alpha) \quad = \quad 0 \tag{3.8}$$

$$y_3^*(1 - \frac{\alpha}{{r_1}^3} - \frac{\mu}{{r_2}^3}) \quad = \quad 0. \tag{3.9}$$

There are five solutions to Eq. (3.8) and Eq. (3.9) which are shown in relation to the location of the binary stars in Fig. 3.1. These five equilibrium positions are most commonly known as the Lagrange points. From Eq. (3.9) we have two basic situations, either $y_3^* \neq 0$ or $y_3^* = 0$. The first of which implies that the terms contained within the parentheses must equal zero which can easily be verified to be satisfied when $r_1 = r_2 = 1$. This means that the planet is the same distance from both stars as the stars are from each other, thus forming an equilateral triangle. We will refer to these points as L_4 and L_5 which have coordinate solutions $<x_3^*,\ y_3^*> = <x_{(4,5)}^*,\ y_{(4,5)}^*>$. Clearly the $x_{(4,5)}^*$ value of these equilateral solutions will be the midway point between the two stars which is

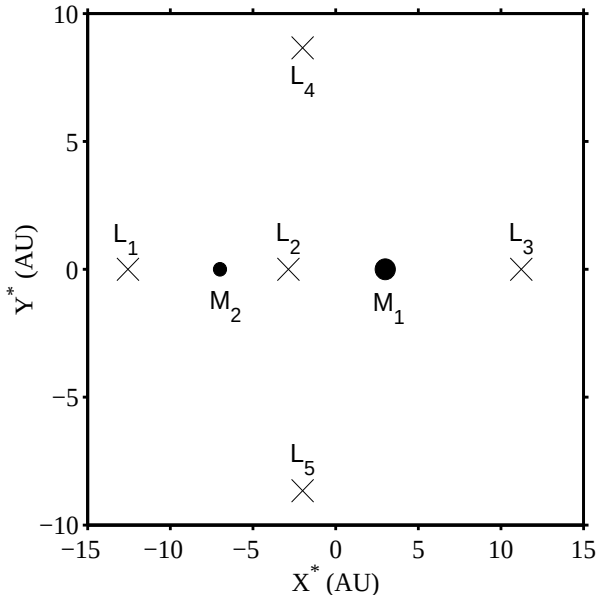

Figure 3.1. The five Lagrange points are shown for the particular case $\mu = 0.3$.

mass ratio dependent. From Eq. (2.14) we can see that the dimensionless position of the stars M_1 and M_2 are μ and $-(1-\mu)$ respectively. It is then easy to see that the midway point of these two positions is $x^*_{(4,5)} = \mu - \frac{1}{2}$. Plugging this back into the equation for either r_1 or r_2 we can easily find that $y^*_{(4,5)} = \pm\frac{\sqrt{3}}{2}$, the plus sign referring to L_4 and the minus sign referring to L_5.

The second situation, $y^*_3 = 0$ implies that any remaining solutions lie on the line passing through the two stars. These collinear points will be designated from left to right by L_1, L_2, L_3 as indicated in Fig. 3.1. These three points cannot be solved for analytically and the numerical method outlined in § 5.8 was used. The location of these points will be useful in distinguishing different regions of motion available to the planet and we will discuss this further in § 3.6

3.3 Jacobi constant at L_4 and L_5

The constant $\overline{C}$ can be set by the initial conditions and the system parameters μ and α, recalling that $\alpha = 1 - \mu$. (See Eq. 3.7) Jacobi's integral is a relationship between the velocity and position of the planet that remains unchanged during the time-dependent development of the system. In the following, we show how using Jacobi's integral at the L_4 and L_5 equilibrium positions can be used to specify the Jacobi constant C, given as $C = \overline{C} + \mu(1 - \mu)$ which has an absolute minimum of $C = 3$ at L_4 or L_5 for any mass ratio.

Since the velocity at L_4 or L_5 is zero and the distance from each star is 1, Eq. (3.7) gives

$$\overline{C}_{(4,5)} \;=\; 2\overline{\phi}_{(4,5)} = r^2 + 2\,(\alpha + \mu) = r^2 + 2\ . \tag{3.10}$$

Since $x^*_{(4,5)} = \mu - \frac{1}{2}$ and $y^*_{(4,5)} = \pm\frac{\sqrt{3}}{2}$, and with $\alpha = 1 - \mu$, we find the planet's distance from the center of mass at L_4 and L_5 is

$$r^2 \;=\; 1 - \mu\alpha. \tag{3.11}$$

This implies that the scalar pseudo-potential $\overline{\phi}_{(4,5)}$ and the constant $\overline{C}_{(4,5)}$ become

$$\begin{aligned} \overline{\phi}_{(4,5)} &= \frac{3}{2} - \frac{1}{2}\mu\alpha \\ \\ \overline{C}_{(4,5)} &= 3 - \mu\alpha\ . \end{aligned} \tag{3.12}$$

Adding $\mu\alpha$ to $\overline{C}$ and adding $\frac{1}{2}\mu\alpha$ to $\overline{\phi}$ does not change the value of Jacobi's integral, and the new constant and pseudo-potential will be the same at L_4 or L_5 for any mass

ratio μ. Therefore, we can define a new pseudo-potential and constant in reference to the equilateral equilibrium points as:

$$\begin{aligned} \phi &= \overline{\phi} + \frac{1}{2}\mu(1-\mu) \\ C &= \overline{C} + \mu(1-\mu) \end{aligned} \tag{3.13}$$

which are valid for any point and not only at L_4 or L_5. Thus, we will refer to C as the Jacobi constant for the remainder of this thesis. Furthermore, with the help of the equation $\alpha r_1^2 + \mu r_2^2 = r^2 + \mu\alpha$, the potential ϕ at any point can be written as

$$\phi = (1-\mu)\Big(\frac{{r_1}^2}{2} + \frac{1}{r_1}\Big) + \mu\Big(\frac{{r_2}^2}{2} + \frac{1}{r_2}\Big). \tag{3.14}$$

We can now rewrite Eq. (3.7) as

$$v^{*2} = 2\phi - C \tag{3.15}$$

and after specifying the initial conditions, the Jacobi constant can be given as

$$C = 2\phi_0 - v_0^{*2}. \tag{3.16}$$

It is worth noting that this is analogous to the energy available to the planet but it is most certainly **not** a statement saying that the energy of the planet is conserved. The total energy of the system is, but if we think back to how Eq. (3.16) was derived, we only considered the potential and kinetic energy of the planet. The potential energy between the stars and their kinetic energies are not a part of this equation.

3.3.1 Extremal value

We already know that the equilateral equilibrium points yield an extreme value of the pseudo-potential, but is it a minimum or a maximum? If we take the first derivative of ϕ (Eq. 3.14) with respect to r_1 and/or r_2 we find that

$$\frac{\partial \phi}{\partial r_i} = k_i \left(r_i - \frac{1}{{r_i}^2} \right) \tag{3.17}$$

where $i = 1, 2$ and $k_i = 1 - \mu, \mu$. We can therefore easily confirm the extremal values of $r_i = 1$ from this. Now if we take the second derivative with respect to r_1 and/or r_2 we find that

$$\frac{\partial^2 \phi}{\partial {r_i}^2} = k_i \left(1 + \frac{2}{{r_i}^3} \right). \tag{3.18}$$

This is always positive for any r_i and ϕ approaches infinity as r_i approaches zero or infinity, so the equilateral equilibrium points are absolute minima and the pseudo-potential and Jacobi constant at these points are:

$$\phi_{min} = \frac{3}{2} \qquad\qquad C_{min} = 3 \tag{3.19}$$

3.4 The Jacobi constant at L_1, L_2, and L_3

Just as the equilateral equilibrium positions served as excellent reference points, the collinear equilibrium positions are useful points of reference for the possible motion allowed to the planet. If a mass were to be stationary at any one of these three points, then we can find the Jacobi constant at such a point from Eq. (3.16) where clearly $v_0^* = 0$ and ϕ_0 is determined at the points L_1, L_2, or L_3. In Fig. 3.2 we show the Jacobi constant for a *stationary* particle lying on the x^* axis for three different mass ratios, $\mu = 0.5$ (red solid line), $\mu = 0.3$ (green dashed line), and $\mu = 0.1$ (blue dash-dotted line). Note that the Jacobi constant diverges as the position approaches either star. These can be considered as *inverted wells* which the planet can be caught in if the Jacobi constant is

sufficiently high. This corresponds to the planet being in orbit around one star or the other. For smaller values of the Jacobi constant, the *wells* become wider until eventually the barrier between the two separate wells no longer exists and the planet is free to move between the two stars. We also recognize that the local minima of the graph correspond to the collinear equilibrium positions. Therefore the middle minimum corresponds to the L_2 point and the value of the Jacobi constant there is C_2. Similarly, the minimum on the left corresponds to L_1 and the one on the right corresponds to L_3.

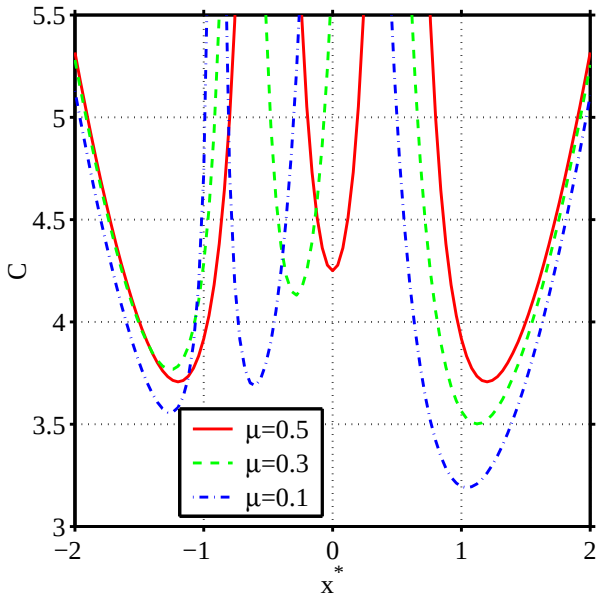

Figure 3.2. The Jacobi constant C as a function of stationary points on the x^* axis.

Clearly, the location of the minimum and the value of the Jacobi constant at these minima is dependent on the mass ratio. Starting with the largest mass ratio considered, we can see that the curves are symmetric when $\mu = 0.5$ which is reasonable since this is when the two stars have equal mass. We can see from the figure that as the mass ratio is reduced from 0.5, the L_3 point moves ever closer to the primary star as C_3 gets smaller and smaller. The L_2 point shifts in the same direction, but it is approaching

the secondary star while C_2 decreases. The L_1 point is a little harder to determine from Fig. 3.2, but it is clear that C_1 has a maximum value at some point. In Fig. 3.3 we show the mass ratio dependence of the Jacobi constant at the three collinear equilibrium points as well as the differences between them. It is now clear that C_1 has a maximum near $\mu = 0.3$ and we numerically find that the maximum occurs at $\mu \approx 0.334$.

If we look at the differences between the Jacobi constants at the collinear points, we can see that the difference between C_2 and C_1 is a nearly linear monotonically increasing function of the mass ratio. This implies that the larger the mass ratio is, the larger the difference between planets that have orbits that can transfer between the stars and planets that have the possibility of being ejected from the system. Thus for the largest mass ratios, initial conditions that give a Jacobi constant that is greater than C_2 and less than C_1 have a good chance of being flung between the stars while still being confined to the inner part of the binary system.

The difference between C_1 and C_3 increases rapidly from $\mu = 0$ and reaches a maximum at $\mu \approx 0.136$, then decreases almost linearly as μ approaches 0.5. It is clear that the difference between C_2 and C_1 is relatively small for μ near 0.136 and this implies that, for μ near this value, there are few initial conditions yielding a Jacobi constant that is greater than C_2 and less than C_1. Therefore, initial conditions that allow the planet to transfer between the two stars are not very far from those that will allow the planet to escape via the opening of the allowable region near the L_1 point.

The difference between C_2 and C_3 represents the relative separation between the L_2 and L_3 points, and the maximum value occurs at $\mu \approx 0.286$, which is fairly close to $\mu \approx 0.334$ which is where the maximum for C_1 is reached.

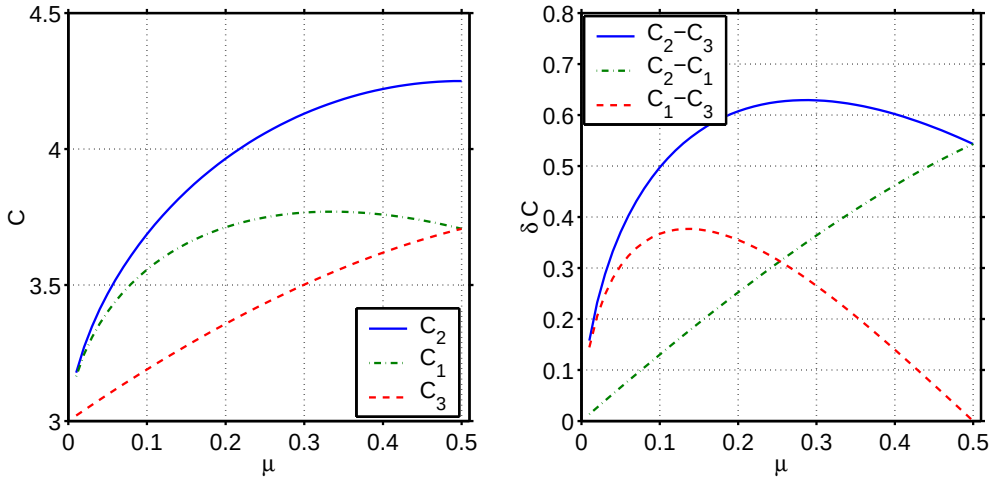

(a) (b)

Figure 3.3. The dependance of the Jacobi constant at the collinear points on the mass ratio μ. (a) Jacobi constant C_1, C_2, and C_3 at the collinear points as a function of mass ratio. Note that C_1 has a maximum at $\mu \approx 0.334$. (b) Differences between collinear Jacobi constants. Note that $C_1 - C_3$ has a maximum for $\mu \approx 0.136$, whereas $C_2 - C_3$ has a maximum for $\mu \approx 0.286$.

3.5 Initial conditions to set the Jacobi constant

In order to find the Jacobi constant for a particular orbit we are interested in, we will need to specify the initial conditions. The planet is started at the three-o-clock position a dimensionless distance of $\rho_0 = R_0/D$ (see Fig. 2.1(a)) relative to the primary star and v_0^* (see Fig. 2.1(b)) is the perpendicular initial velocity of the small body in the rotating coordinate system which will be specified in the next paragraph. The system parameter μ and initial conditions, can now be used to give an expression for the Jacobi constant C, which is

$$C = 2\left[(1-\mu)\left(\frac{{\rho_0}^2}{2} + \frac{1}{\rho_0}\right) + \mu\left(\frac{(1+\rho_0)^2}{2} + \frac{1}{1+\rho_0}\right)\right] - v_0^{*2} \qquad (3.20)$$

The initial velocity is set by adding the initial velocity of the primary star $R_1\omega$ and the velocity that would result in a circular orbit about a stationary star. Therefore, for the initial velocity in sidereal and synodic coordinates, we find

$$\begin{aligned} V_0 &= R_1\omega + \sqrt{\frac{GM_1}{R_0}} \\ V_0^* &= V_0 - (R_1 + R_0)\omega \ , \end{aligned} \tag{3.21}$$

respectively. The dimensionless form of these quantities can be obtained by dividing by $D\omega$, resulting in $v_0 = V_0/D\omega$ and $v_0^* = V_0^*/D\omega$. This also allows us to rewrite v_0 and v_0^* as

$$\begin{aligned} v_0 &= \mu + \sqrt{\frac{1-\mu}{\rho_0}} \\ v_0^* &= \sqrt{\frac{1-\mu}{\rho_0}} - \rho_0 \ . \end{aligned} \tag{3.22}$$

The latter equation allows to express the Jacobi constant C (see Eq. (3.20)) as

$$C = \mu + 2\mu\rho_0 + \frac{1-\mu}{\rho_0} + \frac{2\mu}{1+\rho_0} + 2\sqrt{\rho_0(1-\mu)} \ . \tag{3.23}$$

Obviously, the Jacobi constant solely depends on the system parameters μ and ρ_0, and not on any orbital parameter of the planet, as attained during the simulation, a further indication that C will not change with time.

In Fig. 3.4 we show the Jacobi constant as a function of the initial distance ratio for the various mass ratios considered in this study. The domain chosen for the figure corresponds to the relevant parameter space that was explored because for $\rho_0 \ll 0.2$ we can see that the circular portion of the initial velocity (See Eq. 3.22) will dominate thus the planet is secure in its orbit around the primary star and Eq. (3.23) approaches infinity. There is no question of the stability in this case and in fact the greater C is,

the tighter the orbit of the planet is. Of course in reality the planet cannot orbit with a radius of zero because it would be inside the star so Eq. (3.23) will no longer be valid.

For $\rho_0 > 1.0$ the Jacobi constant continues to increase without bound and the orbit is no longer confined to a satellite type orbit around the primary star (S-type) and it begins to take on a planetary type orbit about both stars (P-type). Again, the greater C is, the more securely the planet is in a circum-binary orbit.

In the intermediate region, $0.2 < \rho_0 < 1.0$ we see that the curves have relative minima and in fact the ρ_0 that are within this interval result in orbits that are difficult to predict the long term behavior of.

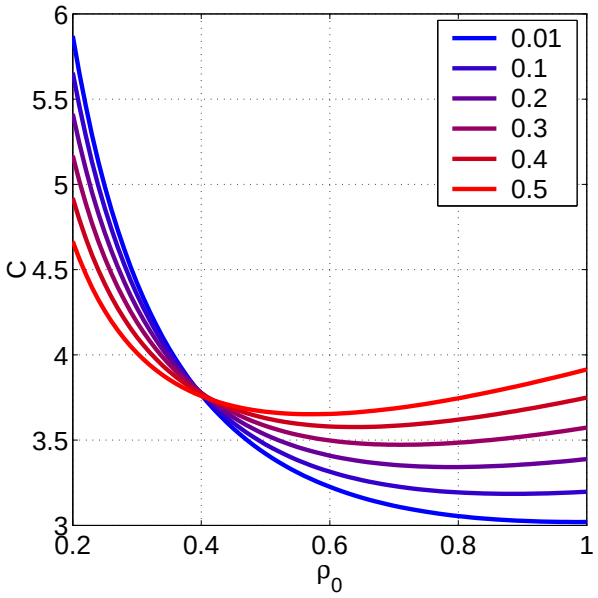

Figure 3.4. The Jacobi constant C as determined by Eq. 3.23 is shown as a function of the initial distance ratio for various mass ratios.

3.6 Zero velocity curves and the allowable regions of motion

Now that C has been set by the initial conditions as described in the previous section, the two terms in Eq. (3.15) will maintain a constant difference, the magnitude of which is just C. Both of these terms, v^{*2} and 2ϕ are always real numbers that are greater than or equal to 0. In the case where $v^{*2} = 0$, then we have $\phi = C/2$. Since ϕ is only a function of position, this allows us to delineate a contour for which the velocity of the planet would have to be equal to zero. If the planet were to somehow move into a region where $\phi < C/2$, then the velocity would be imaginary and this cannot occur. Thus these curves of zero velocity set an allowable region of motion for the planet. The size and shape of the allowable region depends on the initial conditions. From Fig. 3.4, we can see that for relatively small ρ_0 the Jacobi constant is high and therefore from Fig. 3.2, the planet is tightly bound to the primary star. As ρ_0 is increased the Jacobi constant decreases until at one point it is equal to C_2. From this point on, greater values of ρ_0 will give the planet a Jacobi constant that is less than C_2 and then the planet has enough relative energy that it can transfer from the primary star to the secondary star. Just because it *can* does not necessarily mean it *does*. Thus the initial conditions that result in a Jacobi constant that is equal to C_2 are sufficient for an upper limit for "guaranteed stability", but there is not an implication of instability.

As ρ_0 is further increased, the Jacobi constant continues to fall until it is less than C_1. At this point the planet has enough relative energy to escape from the vicinity of the binary stars. It would seem that this would be an adequate way of gauging where instabilities occur. Once again however, just because it *can* escape does not imply that it actually does.

Continuing to increase ρ_0 will further decrease the Jacobi constant until it falls below C_3 at which point the planet can escape from the binaries through an opening that appears in the zero velocity curves near the vicinity of the primary star. This is

a relatively easy escape route and for all but the most robust systems, the planet has become unstable well before reaching this limit.

We didn't investigate the behavior of the system beyond this point because after a moderate increase of ρ_0 the Jacobi constant actually starts to increase (See Fig. 3.4. This implies that the opening near L_3 closes up, and then the opening at L_1 and at this point the planet is excluded from the interior of the binary system. The further out the planet starts its orbit, the more stable this circum-binary orbit is.

3.7 Examples of Orbital Motion and Zero Velocity Curves

In Figs. 3.5, 3.6, and 3.7 we show systems with a mass ratio of 0.5, 0.3, and 0.1, respectively. The initial distance from the primary star is increased as shown and the initial velocity of the planet is set according to Eq. (3.21). The changes to the potential and kinetic energies widen the domain for the possible planetary motion, as implied by the increase of space contained within the zero velocity curves. The space opens up first at the equilibrium point between the two stars. In principle, the planet *could* pass between both stars at this point, but this apparently only happens for the larger mass ratios, as shown in Fig. 3.5.

When the mass ratio is small, the planet remains in a stable, yet peculiar, orbit about the more massive star well beyond the point at which the zero velocity curve has opened up at the L_1 point. This would at least in principle allow the planet to escape the binary system, see Fig. 3.6. Instability seems to occur when the orbit of the planet comes close enough to the zero velocity curve that it abruptly changes direction and falls toward the more massive star, where upon it is catapulted in a new direction and the probability of "disaster" increases. It is difficult to gauge when this is going to occur because there is no obvious way to determine how close the planet has to come to the zero velocity curve for its trajectory to be deflected. As the last part of Fig. 3.7 shows,

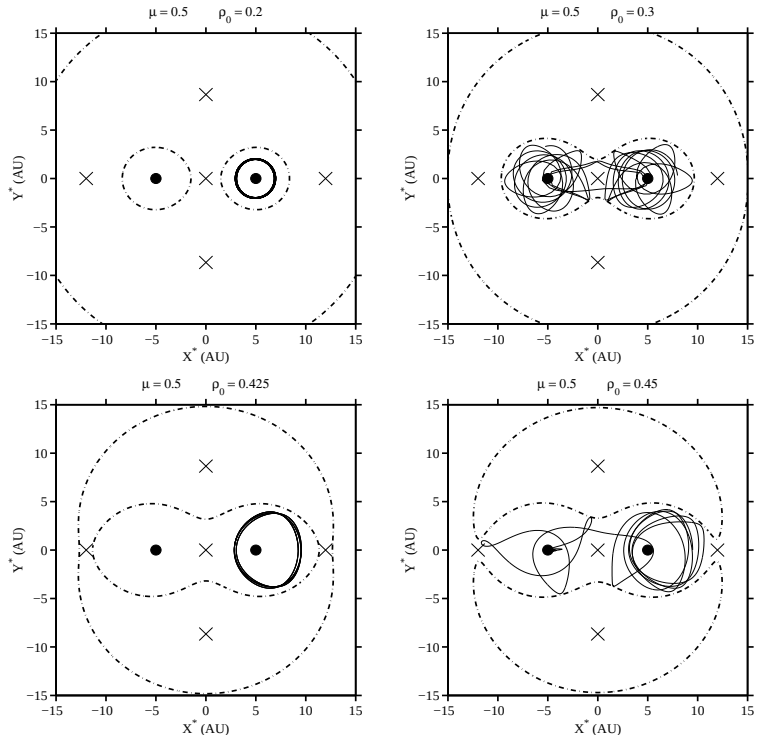

Figure 3.5. For a mass ratio of $\mu = 0.5$, runs for four different distance ratios are shown, which are $\rho_0 = 0.200$, 0.300, 0.425, and 0.450 (solid lines). We also show the borders of the permitted regions of motion (dash-dotted lines) and the Lagrange points.

it could take some time before the planet closely approaches the zero velocity curve and subsequently collides with one of the stars or escapes.

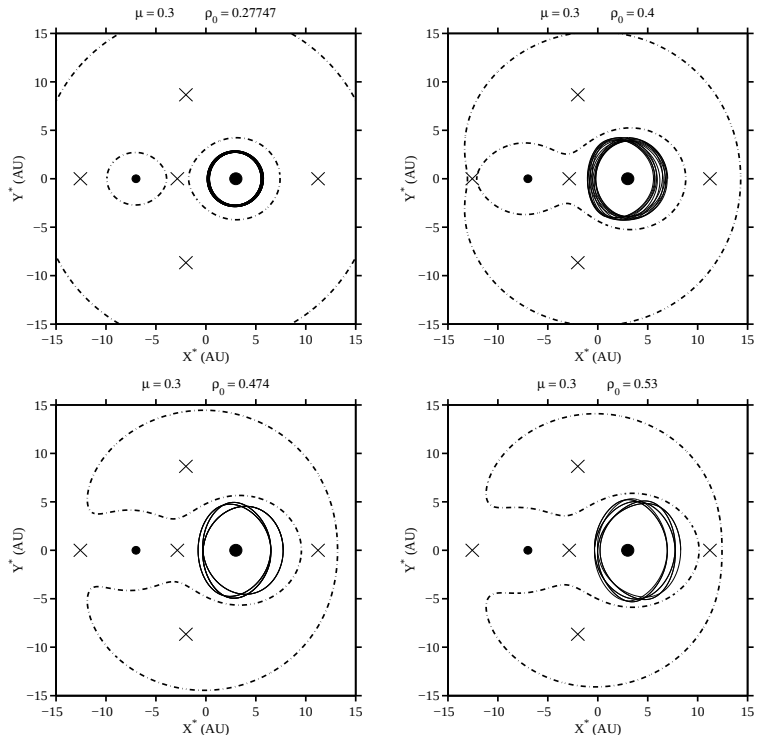

Figure 3.6. Same as Fig. 3.5, but now for a mass ratio of $\mu = 0.3$ and distance ratios of $\rho_0 = 0.277$, 0.400, 0.474, and 0.530.

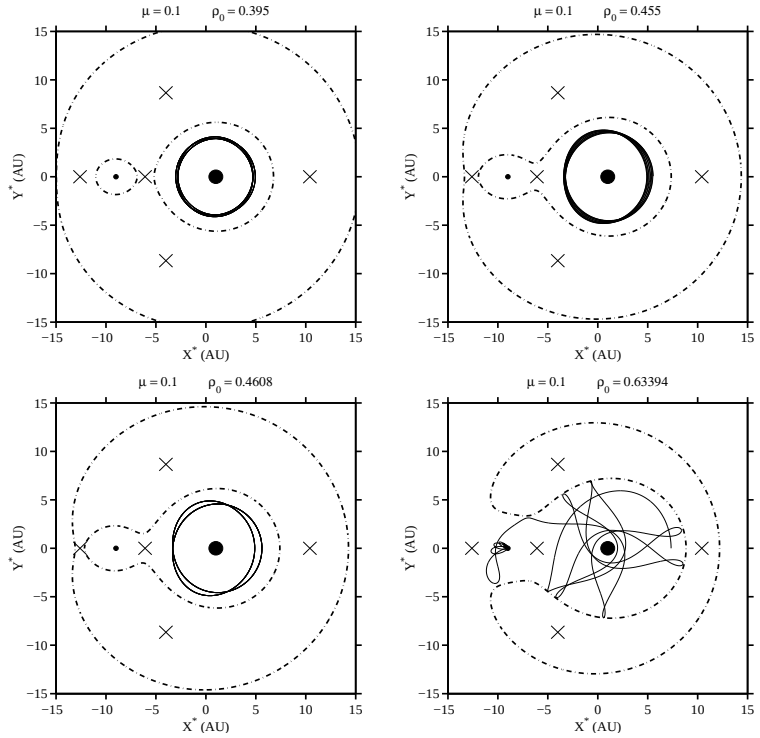

Figure 3.7. Same as Fig. 3.5, but now for a mass ratio of $\mu = 0.1$ and distance ratios of $\rho_0 = 0.395$, 0.455, 0.461, and 0.634.

CHAPTER 4

ESTIMATING STABILITY VIA ECCENTRICITY

In what follows, we show a remarkably simple way to calculate the eccentricity of an orbit at any moment. This will be used as a method of estimating the stability of the orbit later.

4.1 The hodograph of a simple Keplerian orbit

To introduce the method we will start with the orbit of a body in the gravitational field of a single large mass. What we have is just the familiar Kepler orbit with an arbitrary orientation:

$$r \;=\; \frac{p}{1 + e\cos\phi} \tag{4.1}$$

where $\phi = \theta - \theta_0$. Keep in mind that the eccentricity is a constant in this case and can be anything between $0 \leq e < \infty$.

In vector form the position of the planet is:

$$\boldsymbol{r} \;=\; r < \cos\theta, \sin\theta > . \tag{4.2}$$

Now we differentiate with respect to time to obtain the velocity:

$$\boldsymbol{v} \;=\; \frac{r^2}{p}\frac{d\theta}{dt} < -\sin\theta - e\sin\theta_0, \cos\theta + e\cos\theta_0 > . \tag{4.3}$$

Under a central inverse square force, the coefficient in the above equation is constant because $r^2\frac{d\theta}{dt} \;=\; \frac{L}{m} \;=\; h$.

If we were to now plot the components of the velocity vector on a two dimensional plane, then the path the tip of the vector traces out over time is known as a hodograph Hamilton (1847),Butikov (2000).

The velocity vector can be represented by the sum of a vector with constant magnitude $\frac{h}{p}$ rotating about a center with a magnitude from the origin $\frac{he}{p}$:

$$\boldsymbol{v} = \frac{h}{p} < -\sin\theta, \cos\theta > + \frac{he}{p} < -\sin\theta_0, \cos\theta_0 > \tag{4.4}$$

The first term implies that any Kepler orbit will have a hodograph with a fixed radius in velocity space regardless of its eccentricity. The second term implies that any Kepler orbit will also have a hodograph with a fixed center. The ratio of the origin to center "distance" to the magnitude of the constant vector gives us the eccentricity.

Since velocity is orthogonal to position, we can rotate the velocity space clockwise 90 degrees which has the effect of swapping the x and y axes and inverting the x axis which allows an orbit that rotates in the counterclockwise sense to have a velocity vector to rotate in the same sense in velocity space.

In Fig. 4.1 we show the development of the hodograph in relation to the eccentricity of an orbit if the perigee distance is held fixed. The perigee position vector is 1A.U. and the orientation of the orbit is $\theta = \frac{\pi}{4}$. The eccentricity determines the location of the center of the hodograph in relation to its radius in velocity space. If $e < 1$ then we have closed elliptical orbits and the origin of the velocity space coordinate system lies within the hodograph and with the special case of $e = 0$ we have a circular orbit and the center of the hodograph lies on the origin. If $e = 1$ then we have a parabolic orbit and the circular hodograph passes through the origin in velocity space. When $e > 1$ then the orbit is hyperbolic and the radius of the hodograph is less then the distance from its center to the origin. It is worth noting that for closed orbits the hodograph is traced out in one orbital period, while for non-closed orbits it would take an infinite time to fully complete the circle assuming that the planet comes in from infinity and then back out to infinity again. Furthermore, starting from the vicinity of the star, the hodograph

would only trace out a semi-circle in the infinite time it would take for the planet to reach infinity.

If we consider Eq. (4.4), we can see that the term that represents the center also points in the direction of the perihelion. Taking this part of the vector and dividing by the magnitude of the radius of the hodograph, $\frac{h}{p}$, we obtain a vector that gives the orientation of the orbit and has a magnitude equal to e which we will refer to as the eccentricity vector.

4.2 Time varying hodograph in restricted Three Body Problem

In the restricted three body problem we no longer have simple Keplerian orbits with fixed eccentricities. However, we can take small time intervals and approximate the orbit as Keplerian and as such obtain the eccentricity at any given moment. The method used to obtain the eccentricity uses the properties of the hodograph as discussed in the previous section. More specifically, we find the radius of curvature of the hodograph at any given moment by noting that for an arbitrary parameterized function we can find the radius of curvature by the following procedure which can be found in a calculus text such as Stewart (1991). Starting with a parameterized function such as $x = f(t)$ and $y = g(t)$ the curvature is:

$$Q = \frac{(\dot{f}^2 + \dot{g}^2)^{3/2}}{\Lambda} \tag{4.5}$$

and the location of the center point can be calculated as:

$$\xi = f - \frac{(\dot{f}^2 + \dot{g}^2)}{\Lambda}\dot{g} \tag{4.6}$$

$$\eta = g + \frac{(\dot{f}^2 + \dot{g}^2)}{\Lambda}\dot{f} \tag{4.7}$$

where

$$\Lambda = \left| det \begin{pmatrix} \dot{f} & \dot{g} \\ \ddot{f} & \ddot{g} \end{pmatrix} \right| \tag{4.8}$$

and the magnitude of the center from the origin is $O = \sqrt{\xi^2 + \eta^2}$.

If we take $f(t) = v_y$ and $g(t) = -v_x$ then we can see from the previous section that the eccentricity in the synodic frame is $e^* = \frac{O}{Q}$ where we have given the eccentricity a superscript $*$ to distinguish it from an eccentricity in a non-rotating frame.

4.3 Example of time dependent hodographs and eccentricity vector

As an example of what the eccentricity vector can tell us, we look at the particular case of $\mu = 0.1$ with $\rho_0 = 0.461$. This particular initial condition resulted in an interesting periodic orbit so it highlights particularly well the value of the eccentricity vector. In Fig. 4.2, we show the orbit in the synodic frame of reference, the time varying hodograph, the endpoints of the eccentricity vector as calculated from the previous section and a histogram plot of the eccentricity magnitude. We know that the planet is rotating in the counterclockwise direction from previous discussions and we have also mentioned that the velocity space coordinates have been arranged so that the motion of the velocity vector mimics the motion of the planet in coordinate space.

If we keep this in mind while we look at the plot of the eccentricity vector we can see that the eccentricity vector is actually traced out clockwise and the cusps correspond to the relative extremes of the hodograph's curvature. If we count the cusps in the clockwise sense we can see that of the eight distinguishable points, the two that are the furthest to the left are the largest with a magnitude nearly equal to one. This indicates that the planet is closest to being unstable when it passes between the stars and this is to be expected since this is the direction in which the available region of motion has an opening.

Also note that the cusps alternate between pointing in the same direction as the velocity curve and pointing in the *opposite* direction. Since the eccentricity vector points in the direction of the perihelion, it would seem that every other cusp corresponds to an aphelion point. In this regard we could interpret that from cusp to cusp is a half "period", and a full "period" would be between every other cusp. This type of "periodicity" is not the norm and in Fig. 4.3 we show a more typical observation.

Looking at the histograms, we can also see that the relative peaks correspond to the cusps of the eccentricity vector. In Fig. 4.2 we can see fairly well defined peaks whereas in Fig. 4.3 the distribution is more uniform. The size of the peaks in the histogram plot are of course indicative of how often we find that the eccentricity has a particular range of values. We can see that these particular orbits are most often found with fairly low eccentricity, and only briefly have relatively high eccentricity.

4.4 Mean eccentricity as a indication of instability

Recalling that for simple central force motion, the orbit is no longer closed when the eccentricity is greater than or equal to one, by considering the mean value of the eccentricity over the course of the planet's orbit we have a reasonable measure of the planet's stability or instability. Fig. 4.4 shows for each of the mass ratios examined, the obtained mean eccentricity plotted versus the initial distance ratio ρ_0 which is considered representative of the initial conditions. The red vertical line indicates the ρ_0 that yields a Jacobi constant that is equal to C_3. Similarly, the green and blue lines correspond to the initial conditions that yield Jacobi constants equal to C_1 and C_2 respectively. We can clearly see here the expected trend toward greater instability as the planet orbits with larger radii since the eccentricity increases steadily. The gaps that are present for $\mu = 0.4$ and $\mu = 0.5$ are regions in which the planet clearly had an unstable orbit. The initial conditions that yielded mean eccentricities equal to one were taken as the limit of

instability (See Fig. 7.4). The mean eccentricity increases relatively quickly when it is greater than about 0.2 so we could argue that a mean eccentricity of 0.2 is a indication that the orbit is beginning to become less stable.

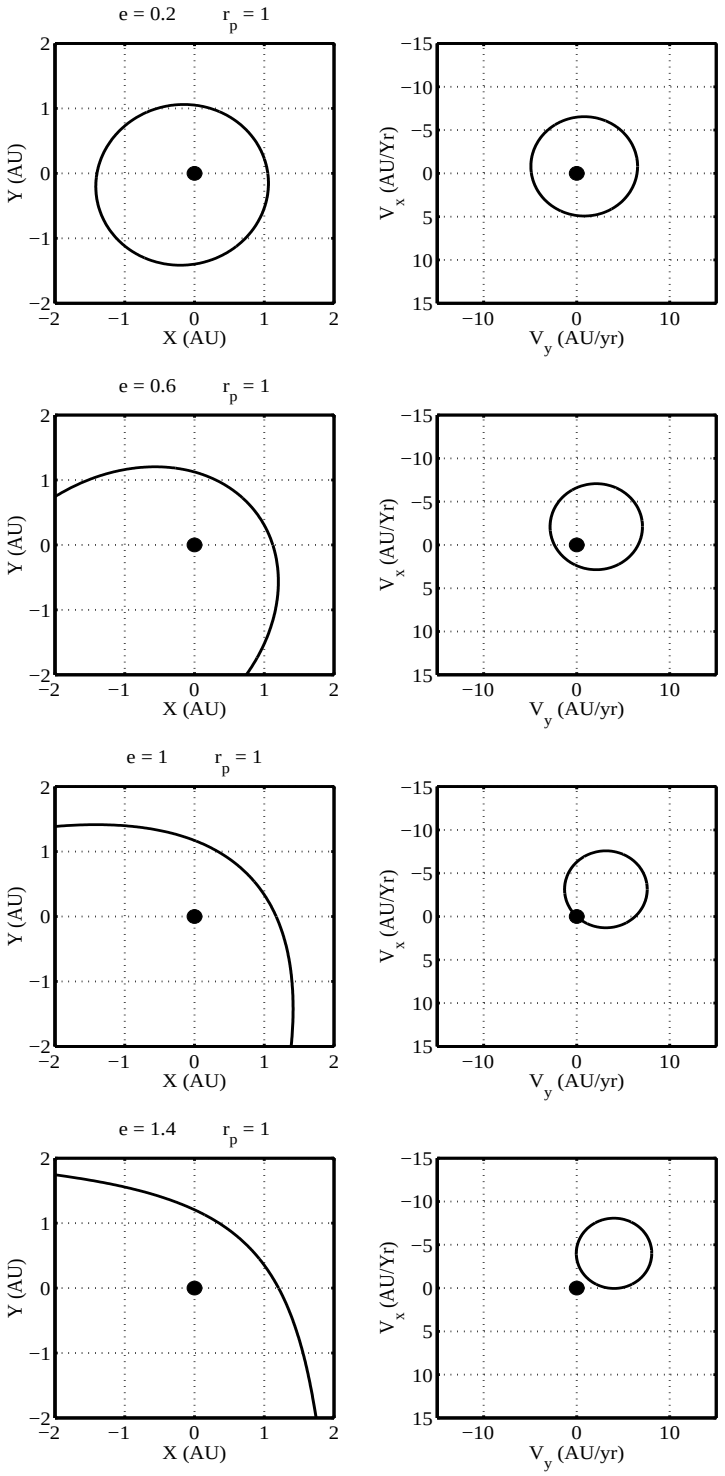

Figure 4.1. Hodograph of a Keplerian orbit. On the left we show Kepler orbits with an orientation of $\pi/4$ and on the right are the corresponding hodographs. The eccentricity is increased from 0.2 to 1.4 in increments of 0.4.

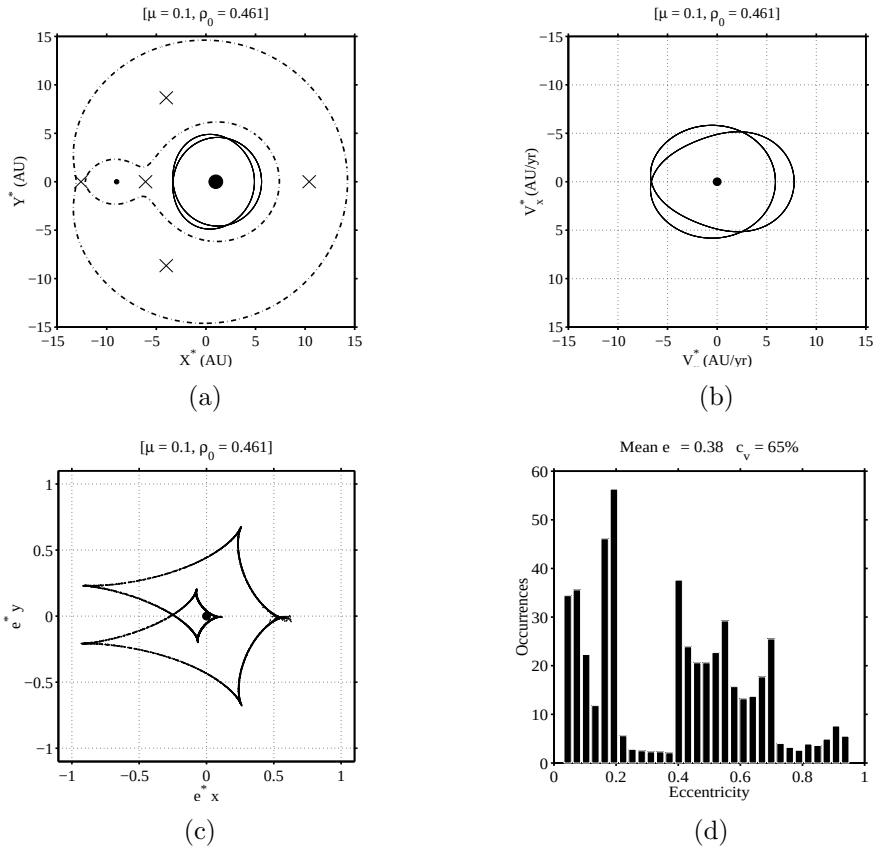

Figure 4.2. For a mass ratio of $\mu = 0.1$ and initial distance ratio of $\rho_0 = 0.461$ the orbit is periodic. We show (a) the orbit of the planet, (b) its hodograph, (c) the path traced out by the eccentricity vector, (d) and the histogram of the eccentricity.

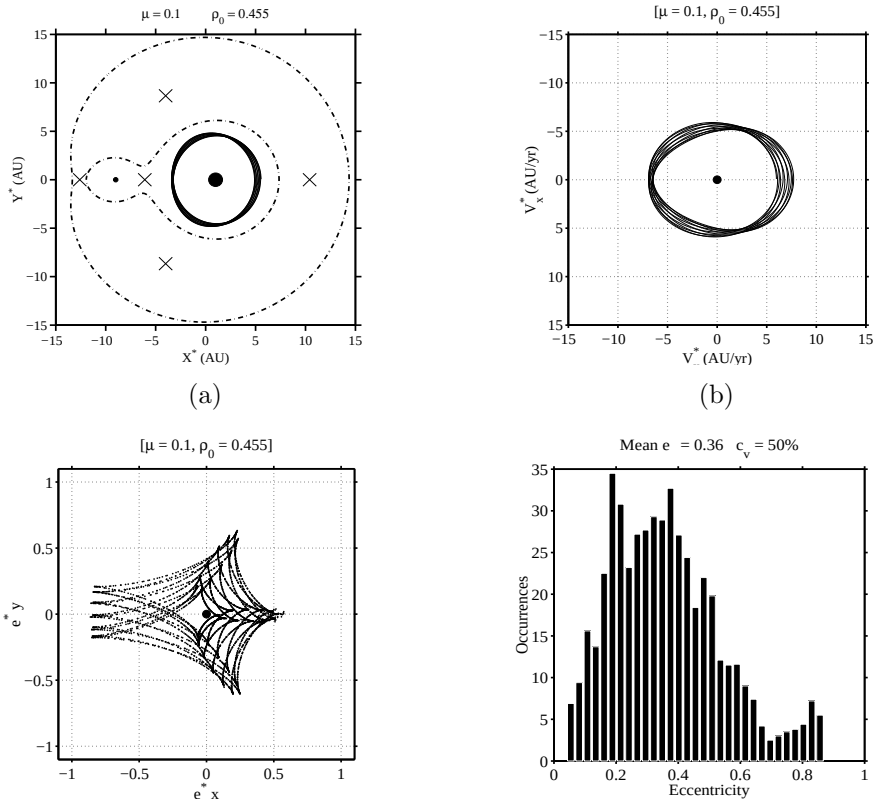

Figure 4.3. For a mass ratio of $\mu = 0.1$ and initial distance ratio of $\rho_0 = 0.455$ the orbit is not periodic. We show (a) the orbit of the planet, (b) its hodograph, (c) the path traced out by the eccentricity vector, (d) and the histogram of the eccentricity.

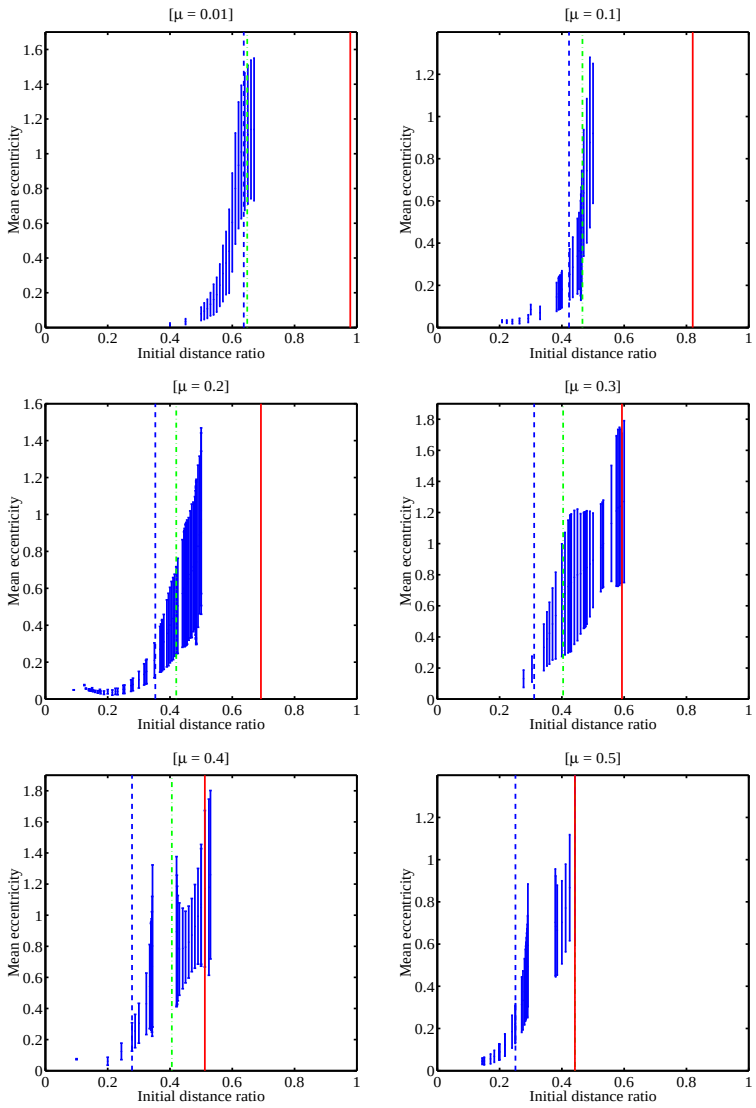

Figure 4.4. The mean eccentricity for various initial conditions. The vertical error bars correspond to the standard deviation.

CHAPTER 5

COMPUTER CODE

5.1 Introduction

As mentioned previously, a 4^{th} order Runge-Kutta integration scheme was used in order to investigate the restricted three body problem. The code used is given in the following sections and was built upon the code given in chapter three of (Garcia 2000) by extending the number of bodies considered from one to three. As can be seen from the following verbatim transcript of the computer code used to integrate the three body problem, there is no implementation of any kind of stability criteria or estimation whatsoever. The only generous escape protocol that was introduced is if the kinetic energy exceeds the magnitude of the potential energy by a factor of two then the program is halted.

5.2 Include files [Nummeth.h]

This file just contains the necessary include statements for the functions that are used in the program. The header file "CBody.h" is defined in the next section.

```
#include <iostream.h>
#include <fstream.h>
#include <stdlib.h>
#include <math.h>
#include <iomanip.h>
#include "CBody.h"
```

5.3 Celestial Body Class [Cbody.h]

This file defines the class CBody which neatly packages all the information about a celestial body such as a star or planet into one data type.

```
//Class for celestial bodies
```

```
#ifndef CBODY_H
#define CBODY_H
class CBody {
    private:
        double normR;
        double normV;
    public:
        CBody(void);
        double state[4+1];
        double tempstate[4+1];
        double accel[2+1];
        double mass;
        double GetR(void);
        double GetV(void);
        void Prepare(void);
        void Update(void);
};
CBody::CBody(void)
{
    for(int i = 1; i<=4; i++)
    {
        state[i] = 0;
        tempstate[i]=0;
    }
    accel[1] = 0;
    accel[2] = 0;
    normR=0;
    normV=0;
    mass=0;
}
double CBody::GetR(void)
{
    normR = sqrt(state[1]*state[1] + state[2]*state[2]);
    return normR;
}
double CBody::GetV(void)
{
    normV = sqrt(state[3]*state[3] + state[4]*state[4]);
    return normV;
```

```
}
void CBody::Prepare(void)
{
    for(int i=0; i<=4; i++)
        tempstate[i] = state[i];
}
void CBody::Update(void)
{
    for(int i=1; i<=4; i++)
        state[i] = tempstate[i];
}
#endif
```

5.4 Derivative function [gravrk.cpp]

```
void gravrk(int p,double t, CBody* param, double deriv[])
{
//  Returns right-hand side of Kepler ODE; used by Runge-Kutta routines
//  Inputs
//    p      number of planet calling function
//    t      Time (not used)
//    param     Pointer to Array of CBody class
//  Output
//    deriv  Derivatives [dr(1)/dt dr(2)/dt dv(1)/dt dv(2)/dt]
const double pi = acos(-1);
double GM = 4*pi*pi;    //magnitude of GM if M = 1
double accelx = 0;
double accely = 0;
double sepex[3+1];      //seperation vectors #: n(n-1)/2 where n = 3 bodies in this case
double sepey[3+1];      //seperated into x and y components
double SEP[3+1];        //magnitude of separation vector
    for(int j=1; j<=3;j++)
    {
    if(j!=p)
    {
        GM = 4*pi*pi*param[j].mass;
        //X-com of separation vector for force on p due to j
        sepex[j] = param[j].tempstate[1]-param[p].tempstate[1];
        //Y-com of separation vector for force on p due to j
```

```
        sepey[j] = param[j].tempstate[2]-param[p].tempstate[2];
        SEP[j]=sqrt(sepex[j]*sepex[j]+sepey[j]*sepey[j]);//magnitude of separation vector
        //* Compute acceleration
        accelx += GM*sepex[j]/(SEP[j]*SEP[j]*SEP[j]);
        accely += GM*sepey[j]/(SEP[j]*SEP[j]*SEP[j]);
    }//if
    }//for
  //* Return derivatives [dr[1]/dt dr[2]/dt dv[1]/dt dv[2]/dt]
  deriv[1] = param[p].tempstate[3];       deriv[2] = param[p].tempstate[4];
  deriv[3] = accelx;   deriv[4] = accely;
```

5.5 Runge-Kutta integrator (4^{th} order) [rk4.cpp]

```
void rk4(int p, double t, double tau,
  void (*derivsRK)(int p, double t, CBody* param, double deriv[]),
  CBody* param)
{
// Runge-Kutta integrator (4th order)
// Inputs
//   p          number of planet calling function
//   t          Independent variable (usually time)
//   tau        Step size (usually time step)
//   derivsRK   Right hand side of the ODE; derivsRK is the
//              name of the function which returns dx/dt
//              Calling format derivsRK(p,t,param,dxdt).
//   param      Extra parameters passed to derivsRK
// Output
//   x          New value of x after a step of size tau
    int i;
    double F1[4+1], F2[4+1], F3[4+1], F4[4+1];
  param[p].Prepare();       //sets tempstate equal to state
  //* Evaluate F1 = f(x,t).
  (*derivsRK)(p, t, param, F1 );    //integrates tempstate
  //* Evaluate F2 = f( x+tau*F1/2, t+tau/2 ).
  double half_tau = 0.5*tau;
  double t_half = t + half_tau;
  for( i=1; i<=4; i++ ) //increments up tempstate
    param[p].tempstate[i] += half_tau*F1[i];
  (*derivsRK)(p, t_half, param, F2 );  //integrates tempstate
```

```
  //* Evaluate F3 = f( x+tau*F2/2, t+tau/2 ).
  for( i=1; i<=4; i++ ) //increments up tempstate
    param[p].tempstate[i] += half_tau*F2[i];
  (*derivsRK)(p, t_half, param, F3 );   //integrates tempstate
  //* Evaluate F4 = f( x+tau*F3, t+tau ).
  double t_full = t + tau;
  for( i=1; i<=4; i++ )
    param[p].tempstate[i] += tau*F3[i];
  (*derivsRK)(p, t_full, param, F4 );
  param[p].Prepare();       //RE-sets tempstate equal to state
  //* Return x(t+tau) computed from fourth-order R-K.
  for( i=1; i<=4; i++ )
  {
    param[p].tempstate[i] += tau/6.*(F1[i] + F4[i] + 2.*(F2[i]+F3[i]));
  }
}
```

5.6 Energy Calculator [energy.cpp]

```
double Kinetic(CBody* param, int i);
double Potential(int n, CBody* param, int i);
double Total(int n, CBody* param);
//  n       the total number of Celestial Bodies
//  param   array of CBody data structures
//  i       index number of a specific body
double Kinetic(CBody* param, int i)
{
double kinetic=0;
    kinetic += 0.5*param[i].mass*param[i].GetV()*param[i].GetV();
    return kinetic;
}//Kinetic
double Potential(int n, CBody* param, int i)
{
const double pi = acos(-1);
double G = 4*pi*pi;
double potential=0;
double sepex[6+1];  //seperation vectors #: n(n-1) where n = 3 bodies in this case
                    //(different directions counted)
double sepey[6+1];  //seperated into x and y components
```

```
double SEP[6+1];    //magnitude of separation vector
for(int j=1; j<=n;j++)
{
if(i!=j)
    {
    //X-com of separation vector for force on i due to j
    sepex[j] = param[j].state[1]-param[i].state[1];
    //Y-com of separation vector for force on i due to j
    sepey[j] = param[j].state[2]-param[i].state[2];
    //magnitude of separation vector
    SEP[j]=sqrt(sepex[j]*sepex[j]+sepey[j]*sepey[j]);
    //adds up total potential of all bodies
    potential+=-G*param[i].mass*param[j].mass/SEP[j];
    }//if
}//for
    return potential;
}//Potential
```

5.7 Main body of code

```
#include "NumMeth.h"
#include "gravrk.cpp"
#include "rk4.cpp"
#include "energy.cpp"
CBody plan[3+1];
void main()
{
int nBodies = 3;
double param [5+1];
int nState = 4;                 //number of elements in state vector
const double pi = acos(-1);     //pi = 3.14159...
double G = 4*pi*pi;             //gravitational constant in Solar Mass, A.U. and year units
double time = 0;
double nStep;
double tau=0;
double r1plot, th1plot, r2plot, th2plot, r3plot, th3plot, r3xplot, r3yplot,
       kinetic, potential, total, tplot, tauplot, p3plot, p3xplot, p3yplot;
//Set up the plotting variables:
//thiplot, riplot, potential, kinetic
```

```
ofstream th1plotOut("th1plot.txt"), r1plotOut("r1plot.txt"),
         th2plotOut("th2plot.txt"), r2plotOut("r2plot.txt"),
         th3plotOut("th3plot.txt"), r3plotOut("r3plot.txt"),
         r3xplotOut("r3xplot.txt"), r3yplotOut("r3yplot.txt"),
         tplotOut("tplot.txt"), tauplotOut("tauplot.txt"),
         potentialOut("potential.txt"), kineticOut("kinetic.txt"),
         p3plotOut("p3plot.txt"), p3xplotOut("p3xplot.txt"), p3yplotOut("p3yplot.txt"),
         ParameterOut("Parameter.txt");
int numData = 5000;                         //prints out 5000 data points
tau = 5e-7;                                 //changed in code for different time steps
nStep = 50/tau;                             //sim duration 50 years
//Dimensions in Solar Masses
    cout<<"Enter mass of primary star in solar mass: ";
    cin>>plan[1].mass;
    cout<<endl<<"Enter mass of secondary star in solar mass: ";
    cin>>plan[2].mass;
    plan[3].mass=1e-6*plan[1].mass;
double d;
    cout<<endl<<"Enter separation of stars in AU: ";
    cin>>d;
    param[5] = d;
double  u = plan[2].mass/(plan[1].mass + plan[2].mass);     //mass ratio
//Dimensions in AU  (center of mass coordinates)
double omega = sqrt(G*(plan[1].mass+plan[2].mass)/(d*d*d));
    plan[1].state[1]=plan[2].mass*d/(plan[1].mass+plan[2].mass);    //Establish the
    plan[1].state[2]=0;                                             //coordinates such
    plan[2].state[1]=plan[1].state[1]-d;                            //that the primary star
    plan[2].state[2]=0;                                             //is on the right
    plan[1].state[3]=0;
    plan[1].state[4]= plan[1].state[1]*omega;  //Circular Orbit
    plan[2].state[3]=0;
    plan[2].state[4]=plan[2].state[1]*omega;
//  The following five lines were used to test code at L4 point.
//  plan[3].state[1] = L[4][0];
//  plan[3].state[2] = L[4][1];
//  double thetan = atan(sqrt(3)/(1-2*u));
//  plan[3].state[3] = -sqrt(L[4][0]*L[4][0] + L[4][1]*L[4][1])*omega*sin(thetan);
//  plan[3].state[4] = -sqrt(L[4][0]*L[4][0] + L[4][1]*L[4][1])*omega*cos(thetan);
    param[0] = 1;       //Type one initial conditions as follows:
```

```
    cout<<"Enter distance of planet from primary star in AU: ";
    cin>>plan[3].state[1];
    param[4] = plan[3].state[1];
//  cout<<endl<<"Enter angle from x-axis for initial velocity: (degrees)";
    double thetan;
    thetan = 90;        //default to 90 degrees for study
//  cin>>thetan;
    //adding the circular velocity about the primary star to the star's initial velocity
    double stitch = sqrt(G*plan[1].mass/fabs(plan[3].state[1])) + plan[1].state[4];
    plan[3].state[2]=0;
    plan[3].state[3]= stitch*cos(thetan*pi/180);
    plan[3].state[4]= stitch*sin(thetan*pi/180);
    cout<<setprecision(5);
    cout<<endl<<"Primary Star mass:     "<<plan[1].mass<<" Mo.";
    cout<<endl<<"Primary Star Orbit radius:  "<<plan[1].state[1]<<" AU.";
    cout<<endl<<"Star velocity: "<<plan[1].state[4]<<" AU/year."<<endl;
    cout<<endl<<"Planet Orbit radius:  "<<plan[3].state[1]<<" AU.";
    cout<<endl<<"Planet velocity: "<<stitch<<" AU/year."<<endl<<endl;
    plan[3].state[1] += plan[1].state[1]; //start planet at proper place
    for(int m=1; m<=3; m++)
        param[m]=plan[m].mass;
cout<<"Simulation time: "<<nStep*tau<<" years"<<endl;
cout<<"# of Steps:      "<<nStep<<" at "<<tau<<" years per step"<<endl;
cout<<"# of Data:       "<<numData<<endl;
cout<<"# of Step/Data:  "<<nStep/numData<<endl;
cout<<"Data separation: "<<nStep/numData*tau<<" Yr"<<endl<<endl;
////////////////////////////////////////////////////////////////////////////////
    ParameterOut<<param[1]<<endl;   //First Mass
    ParameterOut<<param[2]<<endl;   //Second Mass
    ParameterOut<<param[4]<<endl;   //R0
    ParameterOut<<param[5]<<endl;   //D
    ParameterOut<<param[0]<<endl;   //Type of initial conditions
    ParameterOut<<param[3]<<endl;   //small mass
cout<<"Starting simulation,...."<<endl<<endl;
//*****************************************************************************
for(double iStep=1; iStep<=nStep; iStep++)
{
kinetic = 0;
potential = 0;
```

```
total = 0;
                                        //Defined in energy.cpp
    kinetic = Kinetic(plan,3);          //kinetic of body 3
    potential = Potential(nBodies,plan,3);  //potential of body 3
    total = Total(nBodies,plan);        //total energy of system
                                        //returns the kinetic and potential energies
//Record position, velocity and energy for plotting.
if(int(iStep)%int(floor((nStep/numData))) == 0 || iStep == 1)               //REALLY Speeds up the program
{
    cout<<setprecision(5)<<endl;
    cout<<time<<" years: "<<endl;
    cout<<"     KIN: "<<Kinetic(plan,1)<<" "<<Kinetic(plan,2)<<" ";
    cout<<setprecision(3)<<kinetic<<setprecision(5)<<endl;
    cout<<"     POT: "<<Potential(nBodies,plan,1)<<" "<<Potential(nBodies,plan,2)<<" ";
    cout<<setprecision(3)<<Potential(nBodies,plan,3)<<" "<<endl;
    cout<<setprecision(5)<<"        TOT: "<<total<<endl;
if(Kinetic(plan,3)>2*fabs(Potential(nBodies,plan,3)))
{
cout<<"Kinetic Energy is greater then Potential energy by a factor of 2,...no longer bound."<<endl;
cout<<"Possible run-time error or collision....halting simulation."<<endl;
exit(0);
}
///////////////Gets the current state variables///////////////
////////////////////////////////////////////////////////////
r1plot = plan[1].GetR();                                    //
th1plot = atan2(plan[1].state[2],plan[1].state[1]);         //
                                                            //
r2plot = plan[2].GetR();                                    //
th2plot = atan2(plan[2].state[2],plan[2].state[1]);         //
                                                            //
r3plot = plan[3].GetR();                                    //
th3plot = atan2(plan[3].state[2],plan[3].state[1]);         //
r3xplot = plan[3].state[1];                                 //
r3yplot = plan[3].state[2];                                 //
                                                            //
p3plot = plan[3].GetV();                                    //
p3xplot = plan[3].state[3];                                 //
p3yplot = plan[3].state[4];                                 //
                                                            //
```

```
tplot = time;                                                    //
tauplot = tau;                                                   //
                                                                 //
//////////////////////////////////////////////////////////////////
////////////////Then stores them in data files////////////////////
//////////////////////////////////////////////////////////////////
    th1plotOut<<th1plot<<endl;                                   //
    r1plotOut<<r1plot<<endl;                                     //
                                                                 //
    th2plotOut<<th2plot<<endl;                                   //
    r2plotOut<<r2plot<<endl;                                     //
                                                                 //
    th3plotOut<<th3plot<<endl;                                   //
    r3plotOut<<r3plot<<endl;                                     //
    r3xplotOut<<r3xplot<<endl;                                   //
    r3yplotOut<<r3yplot<<endl;                                   //
                                                                 //
    tplotOut<<tplot<<endl;                                       //
    tauplotOut<<tauplot<<endl;                                   //
    potentialOut<<potential<<endl;                               //
    kineticOut<<kinetic<<endl;                                   //
                                                                 //
    p3plotOut<<p3plot<<endl;                                     //
    p3xplotOut<<p3xplot<<endl;                                   //
    p3yplotOut<<p3yplot<<endl;                                   //
                                                                 //
//////////////////////////////////////////////////////////////////
}
    for(int i=1; i<=3; i++)
    {
    plan[i].Prepare();      //sets newstate to state
    //When newstate is passed it is the same as state
    rk4(i, time, tau, gravrk, plan);        //integrate using same timestep
    //Now newstate has been integrated
    }
    for(i=1; i<=3; i++)
    {
    plan[i].Update();   //the idea here is change after all steps are made instead
    }                   //of changing while steps are being made,
```

```
                        //which hopefully reduces error propagation.
                        //doesn't seem to make much difference
    time+=tau;
}// for (iStep=1; iStep<=nStep; iStep++)
}//main
```

5.8 Coordinates and Jacobi constant at the five Lagrange Points

The following is a stand alone program that calculates the coordinates of the five Lagrange points and the value of the Jacobi constant C at these points.

```
#include <iostream.h>
#include <fstream.h>
#include <iomanip.h>
#include <stdlib.h>
#include <math.h>
//  See Szebehely "Theory of Orbits"  Sections 4.3 - 4.4 for algorithm details and derivation
void main(void)
{
double L[5+1][2];
double C[5+1];
double u =0;                //mass ratio
double Lprec = 1e-8;        //desired precision for Lagrange points
double eps=0;               //epsilon term used in derivation of Lagrange points
double oldep =0;            //storage variable for epsilon
double third = 1.0/3;       //just to make things easier
double phi, r1, r2;
ofstream C1Out("C1.txt"), C2Out("C2.txt"), C3Out("C3.txt"),
         C4Out("C4.txt"), C5Out("C5.txt"), uOut("mu.txt");
ofstream L1Out("L1.txt"), L2Out("L2.txt"), L3Out("L3.txt");
    for(u=0.01;u<=0.51;u+=1e-2)
    {
        uOut<<u<<endl;
    //Begin looping for L1...
    eps = pow((u/(3*(1-u))),third);
    do{
    oldep = eps;
    eps = pow(u*pow(1+eps,2)/(3-2*u+eps*(3-u+eps)),third);
    }while(fabs((oldep-eps)/eps)>Lprec);
```

```
L[1][0] = u-1-eps;
L[1][1] = 0;
L1Out<<L[1][0]<<endl;
//Begin looping for L2...
eps = pow((u/(3*(1-u))),third);
do{
oldep = eps;
eps = pow(u*pow(1-eps,2)/(3-2*u-eps*(3-u-eps)),third);
}while(fabs((oldep-eps)/eps)>Lprec);
L[2][0] = u-1+eps;
L[2][1] = 0;
L2Out<<L[2][0]<<endl;
//Begin looping for L3...
eps = 1 - 7.0/12*u;
do{
oldep = eps;
eps = pow((1-u)*pow(1+eps,2)/(1+2*u+eps*(2+u+eps)),third);
}while(fabs((oldep-eps)/eps)>Lprec);
L[3][0] = u+eps;
L[3][1] = 0;
L3Out<<L[3][0]<<endl;
//Simple calculation for L4
L[4][0] = u-0.5;
L[4][1] = sqrt(3)/2;
//Simple calculation for L5
L[5][0] = u-0.5;
L[5][1] =-sqrt(3)/2;
    if(u==0)
        {
            C[1]=3.00;
            C[2]=3.00;
            C[3]=3.00;
            C[4]=3.00;
            C[5]=3.00;
            for(int i=1;i<=5;i++)
            {
                switch(i)
                {
                case 1: C1Out<<C[1]<<endl;
```

```
                    break;
                case 2: C2Out<<C[2]<<endl;
                    break;
                case 3: C3Out<<C[3]<<endl;
                    break;
                case 4: C4Out<<C[4]<<endl;
                    break;
                case 5: C5Out<<C[5]<<endl;
                    break;
                }
            }
        }
    else
        {
            for(int i=1;i<=5;i++)
            {
                r1 = sqrt(pow(L[i][0]-u,2) + L[i][1]*L[i][1]);
                r2 = sqrt(pow(L[i][0]+1-u,2) + L[i][1]*L[i][1]);
                phi = (1-u)*(pow(r1,2)/2 + 1/r1) + u*(pow(r2,2)/2 + 1/r2);
                C[i] = 2*phi;
                switch(i)
                {
                case 1: C1Out<<C[1]<<endl;
                    break;
                case 2: C2Out<<C[2]<<endl;
                    break;
                case 3: C3Out<<C[3]<<endl;
                    break;
                case 4: C4Out<<C[4]<<endl;
                    break;
                case 5: C5Out<<C[5]<<endl;
                    break;
                }
            }
        }
    }//for u loop
}
```

CHAPTER 6

TEST OF COMPUTER CODE

6.1 Stability of L_4 or L_5 points

The accuracy of the computer code is investigated by integrating the equations of motion for a small body placed near the triangular L_4 point. A mass ratio of $\mu = 0.001$ is assumed considering that the triangular Lagrange points are only stable for $\mu \leq \mu_0 = 0.0385 = (1 - \sqrt{69}/9)/2$ as shown in Szebehely (1967). If the small mass is placed near the stable point, it will oscillate about that point. Note that even if in the simulation it could be placed exactly at the stable point, an impossible task owing to truncation errors inherit in any digital variable, the Runge-Kutta integrator would still introduce an error proportional to the size of the time step τ of $O(\tau^5)$ for each step, but $O(\tau^4)$ over multiple steps. This means that smaller time steps will keep the body more closely near the stable point, but will extend the running time of the simulation.

In Table 6.1, it is shown how different values of τ affect the accuracy and running time of the simulation. For smaller time steps the deviation from the equilibrium is smaller; however, the time it takes to run the simulation increases by the same magnitude. The approximate scale of the motion about the stable point is given by the quantity ϵ. T_{sim} is the physical time of the simulation, and T_{run} is the computational time of the simulation to run on a Pentium 4 CPU Dual 3 GHz with 1 GB RAM.

Table 6.1. Tests of computer code

Run	μ	τ [yr step^{-1}]	$T_{\rm sim}$ [yr]	$T_{\rm run}$ [min]	ϵ [AU]
(a)	$1 \cdot 10^{-3}$	$5 \cdot 10^{-6}$	50	10^0	10^0
(b)	$1 \cdot 10^{-3}$	$5 \cdot 10^{-7}$	50	10^1	10^{-1}
(c)	$1 \cdot 10^{-3}$	$5 \cdot 10^{-8}$	50	10^2	10^{-2}
(d)	$1 \cdot 10^{-3}$	$5 \cdot 10^{-9}$	50	10^3	10^{-3}

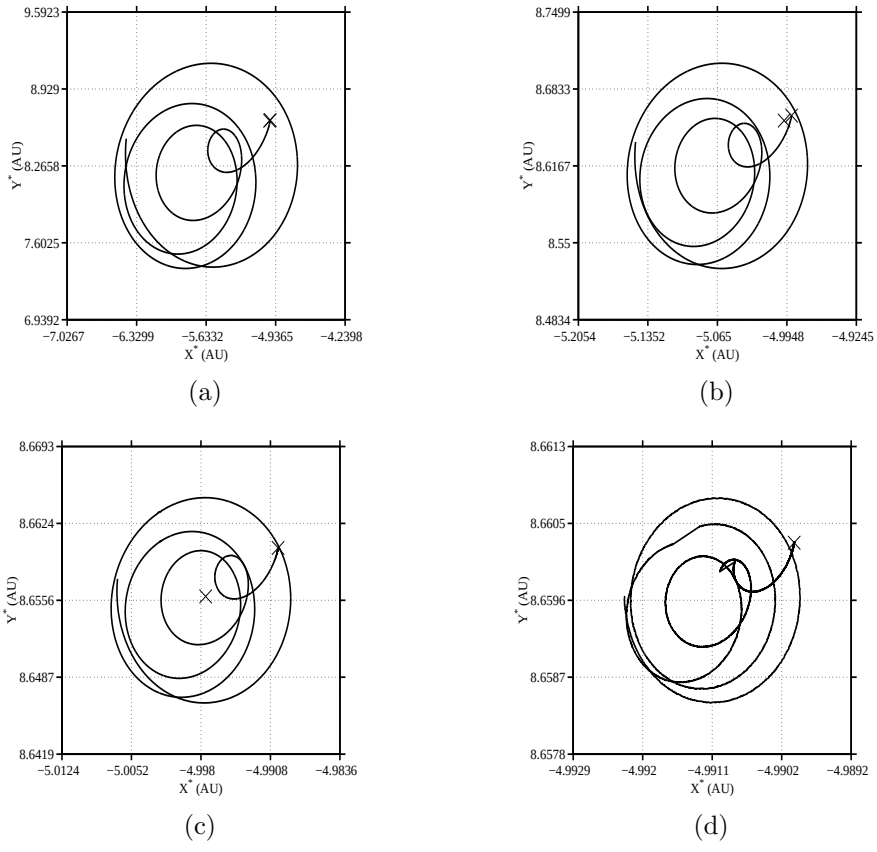

Figure 6.1. For a mass ratio μ of 0.001, the path of the small body near L_4 over the simulation time of 50 years for different time steps τ are shown. (a) $\tau = 5 \times 10^{-6}$, (b) $\tau = 5 \times 10^{-7}$, (c) $\tau = 5 \times 10^{-8}$, (d) and $\tau = 5 \times 10^{-9}$.

CHAPTER 7

RESULTS AND DISCUSSION

7.1 Summary

In Fig. 7.1, we show orbits for $\mu = 0.5$ as the planet is placed further away from the star that it is primarily orbiting, resulting in a decrease in the Jacobi constant (see Eq. (3.23). On the left we show the orbit of the planet in synodic coordinates, in the middle we show the eccentricity vector, and on the right is the eccentricity histogram.

The first part of Fig. 7.1 shows the case $\rho_0 = 0.2$. The eccentricity vector plot is already showing a small deviation from a circular orbit. The next part of Fig. 7.1 shows the limit of stable orbits beyond the L_2 point where $\rho_0 = 0.291$. The orbit of the planet shows an overall progression toward the other star and the eccentricity vector has become highly distorted to the left. It is interesting to note that this part of the plot corresponds to the rightmost extreme of the orbit where it is the closest to the primary star and the eccentricity briefly shoots as high as 2. Upon increasing ρ_0 to 0.292, the orbit becomes unstable within the 50 years of simulation time. This first instability "window" occurs between $\rho_0 = 0.292$ and $\rho_0 = 0.378$.

Eventually, there is a return to stable orbits as the third part of Fig. 7.1 shows the nature of the orbits after passing through the first instability window with a particularly interesting case at $\rho_0 = 0.40$. The eccentricity vector shows a periodic type pattern and it is interesting to see that the eccentricity vector obtains high values on the left and the right in view of the fact that the allowable region for this initial condition is already open at L_2 and is close to opening at L_3. This stability window extends from about $\rho_0 = 0.379$ to 0.43. The final part of Fig. 7.1 shows that the orbits become unstable as

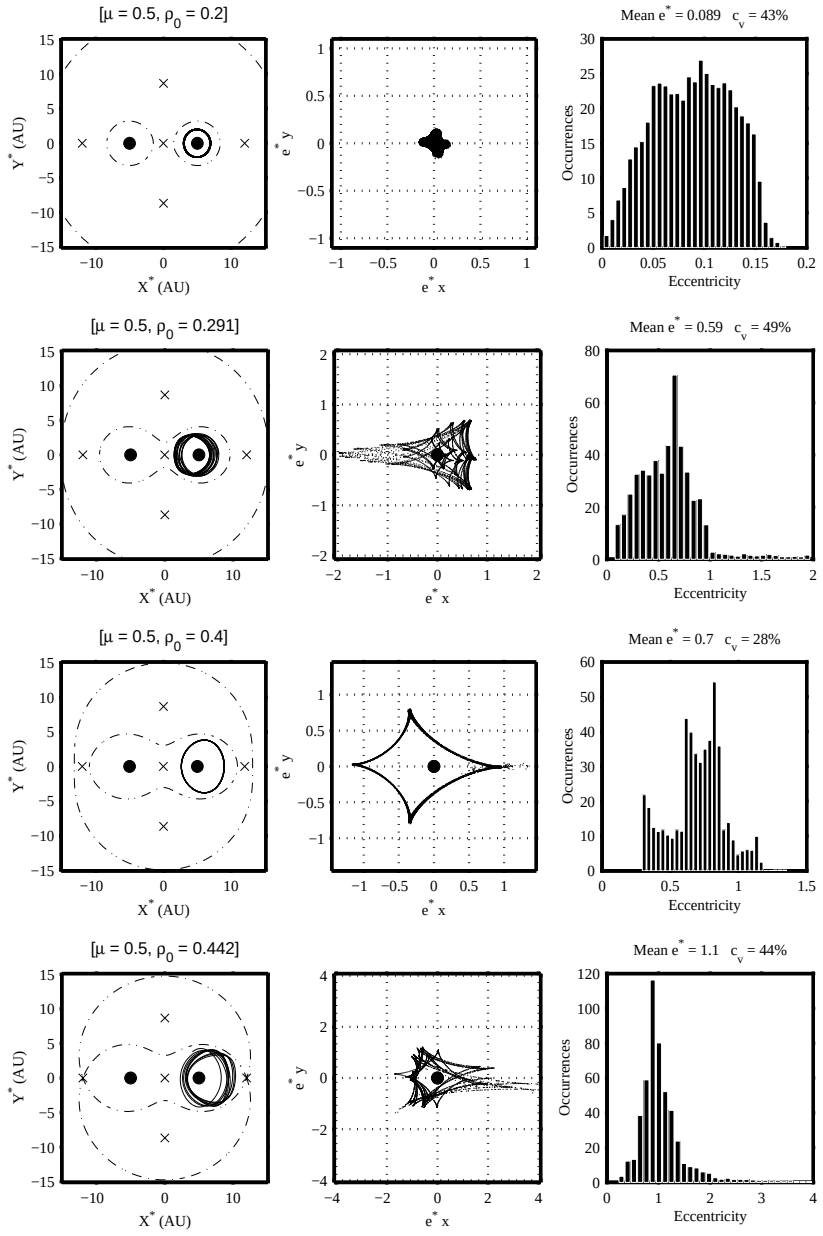

Figure 7.1. For a mass ratio of $\mu = 0.5$, runs for four different distance ratios are shown, which are $\rho_0 = 0.200$, 0.291, 0.400, and 0.442 (solid lines). On the left, we show the orbit of the planet in the synodic coordinate system along with the borders of the permitted regions of motion (dash-dotted lines) and the Lagrange points. In the middle, we show the eccentricity vector and on the right is the eccentricity histogram.

$C \rightarrow C_1 = C_3$. Note the striking similarity of the eccentricity vector plot to the previous instability transition point.

As ρ_0 is increased further, the Jacobi constant eventually reaches a minimum value of 3.652 for $\rho_0 = 0.572$. Beyond this point the allowable region of motion will begin to close up again, until the zero velocity curve passes again through C_3 for $\rho_0 = 0.740$. This prevents the planet from approaching the region near the stars, at least from the right. We refrained from investigating initial conditions beyond a certain point because the orbit no longer returned to a stable S-type orbit.

Since the development of $\mu = 0.4$ is almost identical to that just described, only the distinguishing aspects will be mentioned (see Table 7.1). The main distinguishing points between $\mu = 0.5$ and 0.4 is that for $\mu = 0.5$, the stability window starts prior to reaching C_1 and becomes unstable again before reaching C_3, while for $\mu = 0.4$ the stability window starts after reaching C_1 and becomes unstable soon after reaching C_3. These differences are likely due to the fact that for $\mu = 0.5$, $C_1 = C_3$ and for $\mu = 0.4$, $C_1 > C_3$.

We can see from Fig. 7.2 that the development for $\mu = 0.3$ is similar and the eccentricity again is a maximum when the planet passes between the two stars. What is significantly different here is that even though the eccentricity obtains relatively large values that would be considered hyperbolic, the orbit of the planet is at least quasi-stable. It is as though the planet is trying to escape, but the zero velocity curve is keeping it rounded up. Once again however, when the Jacobi constant approaches C_3, the eccentricity grows large towards the opening at L_3 and the orbit is unstable.

In Fig. 7.3 we show the development for $\mu = 0.1$ from the limit of stability to the limit of instability which is a relatively small interval. It is interesting to note that even though the mean eccentricity remains low, the eccentricity peaks to nearly one as it passes between the stars as can be seen for the case $\rho_0 = 0.461$. As ρ_0 is increased a

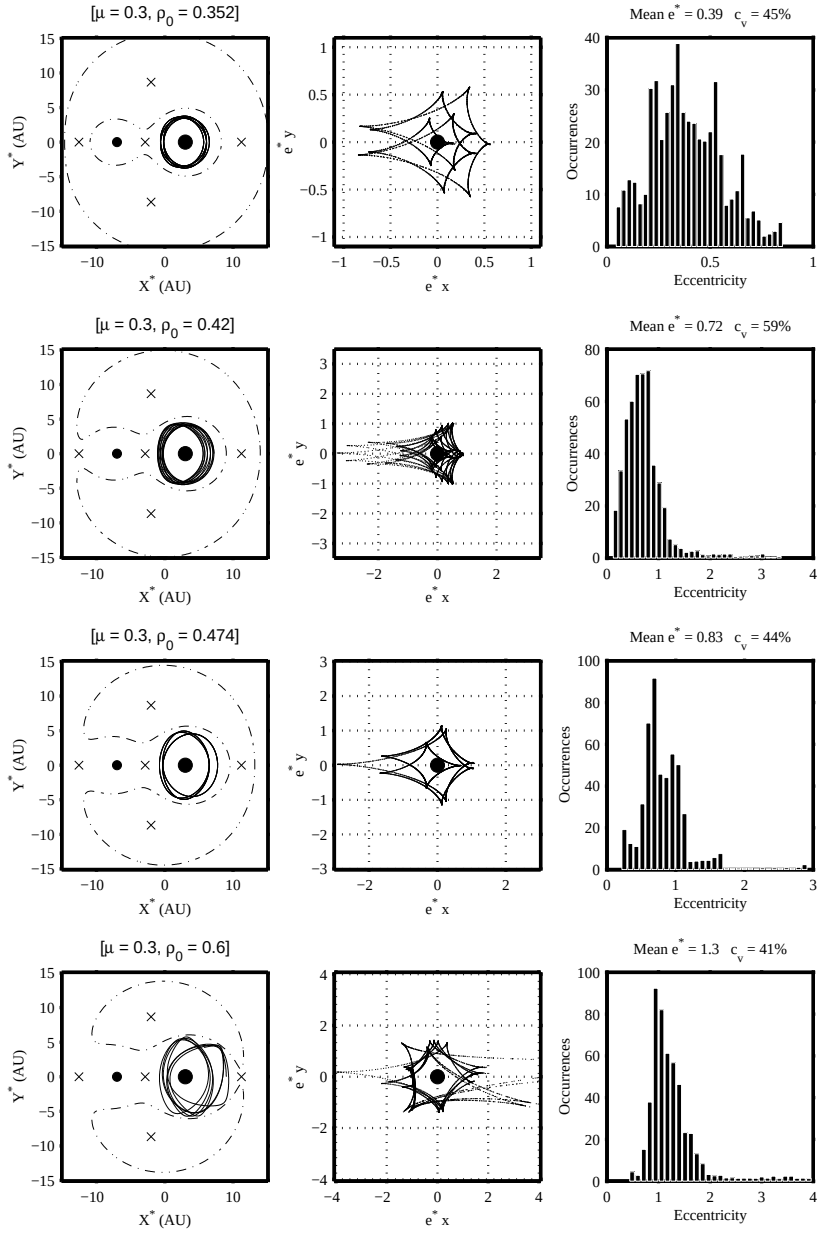

Figure 7.2. Same as Fig. 7.1, but now for a mass ratio of $\mu = 0.3$ and distance ratios of $\rho_0 = 0.352$, 0.420, 0.474, and 0.600.

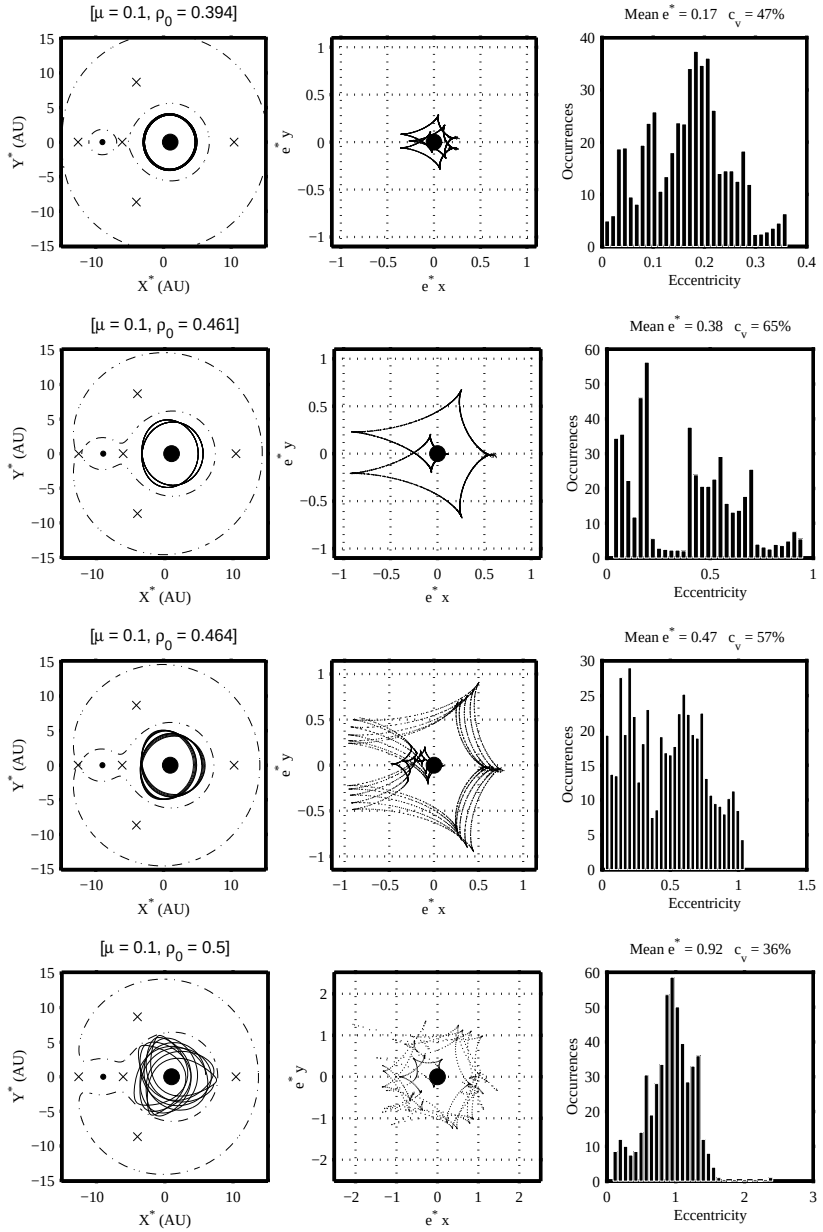

Figure 7.3. Same as Fig. 7.1, but now for a mass ratio of $\mu = 0.1$ and distance ratios of $\rho_0 = 0.394$, 0.461, 0.464, and 0.500.

Table 7.1. Stability regimes for different mass ratios μ

μ	$\rho_0 \rightarrow C_2$	$\rho_0 \rightarrow C_1$	$\rho_0 \rightarrow C_3$	Unstable	Quasi-Stable
0.50	0.251	0.442	0.442	$0.29 \rightarrow 0.38$	$0.38 \rightarrow 0.43$
0.40	0.278	0.406	0.512	$0.34 \rightarrow 0.42$	$0.42 \rightarrow 0.52$
0.30	0.311	0.404	0.593	...	$0.31 \rightarrow 0.53$
0.20	0.353	0.420	0.692	...	$0.35 \rightarrow 0.48$
0.10	0.423	0.466	0.820	...	$0.42 \rightarrow 0.46$
0.01	0.637	0.648	0.979	...	$0.64 \rightarrow 0.66$

little more, it appears that the orbit is becoming unstable but the mean eccentricity is still less than one. It would seem that the value of the eccentricity as the planet passes between the stars is more indicative of when instability occurs for the smaller mass ratios, but this requires further investigation. However, we can see that even when the orbit is clearly becoming unstable for $\rho_0 = 0.5$, the mean eccentricity is approaching one.

In Table 7.1 we show the ρ_0's that result in Jacobi constants equal to C_2, C_1, and C_3. In addition, we show initial conditions that result in Unstable and Quasi-Stable intervals. There is an implied quasi-stable interval between the ρ_0 that gives C_2 and the lower bound for the unstable interval for the two highest mass ratios. For example, for $\mu = 0.5$, there is an implied quasi-stable interval between $\rho_0 = 0.251$ and 0.29.

Table 7.1 depicts the general development of the system for the various cases studied. As μ is decreased, the value of ρ_0 that results in the zero velocity curve passing through the L_2 point, C_2 increases. This can be interpreted as an increasing range of "guaranteed" stability. In addition, the interval of quasi-stability increases until a maximum interval for about $\mu = 0.3$ is reached. Thereafter, the interval of quasi-stability decreases rapidly. This can perhaps be explained in terms of the difference between C_2 and C_3 which has a maximum at $\mu = 0.286$ and the maximum for C_1 at $\mu = 0.334$ as mentioned in Fig. 3.3.

For $\mu < 0.3$, there is neither an instability window between C_2 and C_1, nor in the interval between C_1 and C_3. Since the orbital stability is ensured if $C > C_2$, we will use the initial conditions corresponding to $C = C_2$ as a lower bound for the "quasi-stable" region for $\mu < 0.3$ (see Table 7.1). The development of the orbits for the smaller mass ratios is a more continuous evolution from circular orbits if $C \gg C_2$ to the stable periodic or quasi-periodic orbits in the range where $C_1 < C < C_2$.

For the smaller mass ratios, the difference between C_2 and C_1 is very small and consequently the initial conditions that result in zero velocity curves passing through the L_2 and L_1 points are close together. It should also be noted that as the mass ratio approaches zero, the values of C_2 and C_1 approach each other much more quickly than C_3. This implies that even though the range of initial conditions for which $C > C_2$ is large, once C_2 is passed, the transition to instability occurs well prior to $C \to C_3$.

For the larger mass ratios the difference between C_2 and C_1 is relatively large and consequently the initial conditions that result in zero velocity curves passing through the L_2 and L_1 points are widely spaced. It is worth pointing out that the instability windows occur in this interval as well. Furthermore, the difference between C_1 and C_3 is very small and accordingly the initial conditions that result in zero velocity curves passing through the L_1 and L_3 points are close together.

7.2 Comparison to previous work

The stability limit as considered at the point where the Jacobi constant is equal to C_2 agrees well with the work done by others such as Holman and Wiegert (1999) and Musielak et al. (2005). Holman and Wiegert give a least-squares fit for their stability criteria that relates the distance between the primary star and the planet to the mass ratio and eccentricity of the binary star system. If we consider this equation in terms of

our variables and let the binary eccentricity equal 0 for a circular orbit we get the simple relation:

$$\rho_0 = 0.464 - 0.380\mu \tag{7.1}$$

This is a simple linear equation and the line is shown in Fig. 7.4 along with the lines separating stability, marginal stability, and instability (from left to right) obtained by Musielak et al. (2005). We also show the curve that relate the distance ratio and mass ratio for where the zero velocity curves pass through the L_2 and L_1 points. Also shown are the initial conditions which gave a mean eccentricity of 0.2 (closed circles) and 1.0 (open circles).

The boundary line between stability and marginal stability as obtained by Musielak et al. (2005) agrees very well with the curve corresponding to C_2. The points where the mean eccentricity is equal to 0.2 matches up with the same curve very well too.

There is less agreement for the instability limits and there is probably a simple explanation for this. Most computer simulations being carried out are for very long time scales and the goal is to determine how long it takes before a planet (or a population of planets) is ejected from the system or falls into a star. The simulations carried out in this thesis were only over a very small time scale and thus the limits of instability (mean eccentricity equal to one) represent the limit of short time scale instabilities. There is no question that if longer time intervals were considered, then the instability limit would shift toward smaller distance ratios.

Everything considered in this thesis depends on the fact that the stars are orbiting each other in a circle. As we mentioned earlier, the problem is more difficult if the stars orbit each other in an ellipse; the eccentricity of the stars orbit around each other can be anything between 0 and 1. The constant of motion that we were able to use to describe the

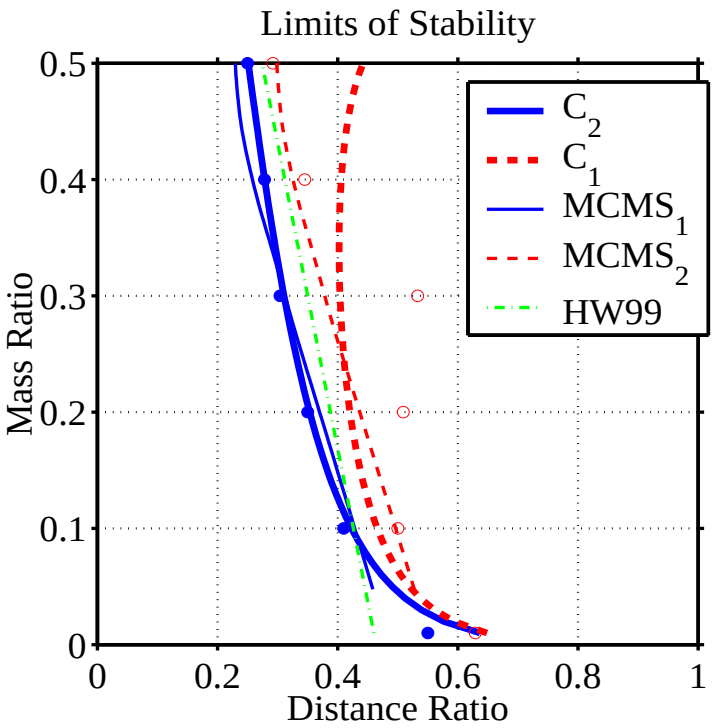

Figure 7.4. Limits of stability for planetary orbits for different mass ratios μ. We show the result based on Jacobi's constant C_2 (thick solid blue line) (criterion of stability) and as comparison Jacobi's constant C_1 (thick dashed red line). We also show the divide obtained by the eccentricity criterion $e = 1.0$ (open red circles) (criterion of instability) and $e = 0.2$ (closed blue circles), with the latter fitting very well the run given by Jacobi's constant C_2. For comparison, we show the regions of stability, marginal stability, and instability (from left to right) previously obtained by Musielak et al. (2005), depicted by thin solid blue and thin dashed red lines. The stability limit from the earlier work by Holman and Wiegert (1999) is depicted as thin dash-dotted green line.

available region of motion no longer exists in the elliptical problem, but we can define a non-uniformly rotating and pulsating coordinate system in which the stars would remain at rest and the "constant" of motion would now be a function of time and the allowable region would pulsate along with the orbit of the stars which is discussed in the final chapter of Szebehely (1967). The method of using the eccentricity vector could also be adapted to the elliptical restricted three body problem in an attempt to define stability boundaries. Furthermore, the numerical integration carried out in this study used a fixed

time step. Since the rate at which the stars orbit each other in an elliptical system is variable, a fixed time step integrator would not be well suited to such an investigation. A variable time step integrator would be required and this would further complicate the problem. The difficulties involved are well worth taking on since real binary systems are elliptical and not circular. The number of extra solar planetary systems continues to rise and there are still many questions as to how these systems form. Knowing how planets form in single or multiple star systems, and whether they have stable orbits or not is fundamental to our understanding of our place in the universe.

Bibliography

G. Á. Bakos, R. W. Noyes, G. Kovács, D. W. Latham, D. D. Sasselov, G. Torres, D. A. Fischer, R. P. Stefanik, B. Sato, J. A. Johnson, A. Pál, G. W. Marcy, R. P. Butler, G. A. Esquerdo, K. Z. Stanek, J. Lázár, I. Papp, P. Sári, and B. Sipöcz. Hat-p-1b: A large-radius, low-density exoplanet transiting one member of a stellar binary. *Astrophysical Journal*, 656:552–559, 2007.

M. Bonavita and S. Desidera. The frequency of planets in multiple systems. *Astronomy and Astrophysics*, 2007.

Eugene. I. Butikov. The velocity hodograph for an arbitrary keplerian motion. *European Journal of Physics*, 21:297–302, 2000.

A. Chenciner and R. Montgomery. A remarkable periodic solution of the three-body problem in the case of equal masses. *Annals of Mathematics*, 152:881–901, 2000.

Eva-Marie David, Elisa V. Quintana, Marco Fatuzzo, and Fred C. Adams. Dynamical stability of earth-like planetary orbits in binary systems. *Publications of the Astronomical Society of the Pacific*, 115:825–836, 2003.

A. Duquennoy and M. Mayor. Multiplicity among solar-type stars in the solar neighbourhood. *Astronomy and Astrophysics*, 248:485–524, 1991.

R. Dvorak. Critical orbits in the elliptical restricted three-body problem. *Astronomy and Astrophysics*, 167:379–386, 1986.

A. Eggenberger, S. Udry, and M. Mayor. Statistical properties of exoplanets. *Astronomy and Astrophysics*, 417:353–360, 2004.

Marco Fatuzzo, Fred C. Adams, Richard Guvin, and Eva M. Proszkow. A statistical stability analysis of earth-like planetary orbits in binary systems. *Publications of the Astronomical Society of the Pacific*, 118:1510–1527, 2006.

Alejandro L. Garcia. *Numerical Methods for Physics*. Prentice-Hall, Inc., Upper Saddle River, New Jersey, second edition, 2000.

William Rowan Hamilton. In *Proceedings of the Royal Irish Academy*, volume 3, pages 344–353. Royal Irish Academy, 1847. transcribed and edited by David R. Wilkins http://www.maths.soton.ac.uk/EMIS/classics/Hamilton/Hodo.pdf, 2000.

Matthew J. Holman and Paul A. Wiegert. Long-term stability of planets in binary systems. *The Astronomical Journal*, 117:621–628, 1999.

W. Kley. Planet Formation in Binary Systems. In H. Zinnecker and R. Mathieu, editors, *The Formation of Binary Stars*, volume 200 of *IAU Symposium*, pages 511–518, 2001.

M. Konacki. An extrasolar giant planet in a close triple-star system. *Nature*, 436:230–233, July 2005. doi: 10.1038/nature03856.

J. Laskar. Chaos in the solar system, 2002. http://www.imcce.fr/fr/presentation/equipes/ASD/preprints/prep.2003.

Lawrence R. Mudryk and Yanqin Wu. Resonance overlap is responsible for ejecting planets in binary systems. *Astrophysical Journal*, 639:423–431, 2006.

Zdislaw E. Musielak, Manfred Cuntz, E. A. Marshall, and T. D. Stuit. Stability of planetary orbits in binary systems. *Astronomy and Astrophysics*, 434:355–364, 2005.

J. Patience, R. J. White, A. M. Ghez, C. McCabe, I. S. McLean, J. E. Larkin, L. Prato, Sungsoo S. Kim, J. P. Lloyd, M. C. Liu, J. R. Graham, B. A. Macintosh, D. T. Gavel,

C. E. Max, B. J. Bauman, S. S. Olivier, P. Wizinowich, and D. S. Acton. Stellar companions to stars with planets. *Astrophysical Journal*, 581:654–665, 2002.

E. V. Quintana, J. J. Lissauer, J. E. Chambers, and M. J. Duncan. Terrestrial planet formation in the alpha centauri system. *Astrophysical Journal*, 576:982–996, 2002.

Archie E. Roy. *Orbital Motion*. Institute of Physics Publishing, London, fourth edition, 2005.

James Stewart. *Calculus*. Brooks/Cole Publishing Company, Pacific Grove, California, second edition, 1991.

Gerald Jay Sussman and Jack Wisdom. Chaotic evolution of the solar system. *Science*, 257(5066):56–62, 1992.

Keith R. Symon. *Mechanics*. Addison-Wesley, Reading, Massachusetts, third edition, 1971.

Victor G. Szebehely. *Theory of Orbits*. Academic Press, New York and London, first edition, 1967.

D. E. Trilling, J. A. Stansberry, K. R. Stapelfeldt, G. H. Rieke, K. Y. L. Su, R. O. Gray, C. J. Corbally, G. Bryden, C. H. Chen, A. Boden, and C. A. Beichman. Debris disks in main-sequence binary systems. *The Astrophysical Journal*, 658:1289–1311, 2007.

BIOGRAPHICAL STATEMENT

William Jason Eberle was born in Reading, Pennsylvania, in 1976. He received his B.S. in Physics from the University of Texas at Dallas, in 2004, and his M.S. in Physics from The University of Texas at Arlington in 2007. He became interested in the gravitational three body problem during his junior year at UTD and has worked on it in his spare time ever since. To have been able to compose his thesis on this pet project of his was unexpectedly fortunate. Jason become interested in complexity theory, chaos, and astrobiology while at UTA. He is in the very early stages of designing a physics simulation and visualization program which will most likely become his pet project for the foreseeable future.